hydroxytoluene (BHT). Under these conditions, we have previously shown that LDL oxidation does not proceed further at 4°C. As LPS could activate MAPK and induce Cox-2, we assessed LPS contamination in our lipoproteins using the endotoxin kit by Sigma (Italy) according to the manufacturer's instructions, no contamination was detected (data not shown). Native LDL and Ox-LDL were used within 6 h from preparation.

Cells. Human umbilical vein endothelial cells (HUVEC) were isolated as described (31), cultured under standard conditions in medium M-199 containing 20% FCS (fetal calf serum), heparin (15 U/ml) and ECGF (endothelial cell growth factor, 20 μg/ml) (Roche, Italy) and used within the 4th passage. Cells were plated in 6-well plates and used as sparse cultures. In all the experiments, cells were pre-incubated with serum-free medium for 6 h and then n-LDL or Ox-LDL were added.

Antibodies. The rabbit polyclonal phospho-p38 MAPK antibody specific for dual-phosphorylated ^{180}Thr and ^{182}Tyr of p38 MAPK and the mouse monoclonal phospho-p44/42 MAPK antibody specific for dual phosphorylated ^{202}Thr and ^{204}Tyr of p44 and p42 MAP kinases were from New England Biolabs (Germany). Monoclonal antibodies against Cox-1 and Cox-2 were from Cayman (USA). Monoclonal antibody anti-ß-actin was from Sigma. Peroxidase-conjugated anti-mouse IgG was from Sigma and peroxidase-conjugated anti-rabbit IgG was from BioRad (Italy).

MAPK and Cox-2 selective inhibitors. The MEK1 inhibitor, PD98059 (New England Biolabs) has been shown to act *in vivo* as a highly selective inhibitor of MEK1 and the ERK1/ERK2 cascade (11). Cells were pre-treated for 1 h with PD98059 at 25 μM. The p38 MAPK inhibitor SB203580 (Sigma) (7) was used at a final concentration of 0.5 μM. Indomethacin heptyl ester (Cayman), a selective Cox-2 inhibitor (32) was used at 0.1 μM. Cells were pre-treated for 1 h with these compounds, lipoproteins were then added.

Immunoblotting. Cellular proteins were collected and electrophoresed as described (33). The membranes were incubated with primary antibody (1:1000 incubation at 4°C overnight for phospho-p38 MAPK and phospho-p44/42 MAPK antibodies; 1:1000 incubation at room temperature for 1 h for Cox-1 and Cox-2 antibodies; 1:1000 incubation at room temperature for 1 h for the ß-actin antibody), followed by a 1:1000 dilution of peroxidase-conjugated anti-mouse IgG (Sigma) or peroxidase-conjugated anti-rabbit IgG (BioRad). Immunocomplexes were detected by an enhanced chemiluminescence method (ECL, Amersham, Italy), followed by autoradiography and quantified by the Image program (NIH 1.52).

Immunocytochemistry. Cells were cultured on coverslips in 24-well plates ($1.5x10^4$ cells/well). After incubation with Ox-LDL, the media were removed and the cells were fixed with 3% paraformaldehyde for 20 min, washed twice with PBS and a solution of 0.2% Triton X100 was added for 2 min at 4°C. After washing twice with PBS, fixed cells were incubated with a monoclonal antibody for Cox-2 (1:20) overnight at 4°C. As a second antibody, an anti-mouse IgG FITC-conjugated (1:100, RD) was used for 30 min, followed by incubation with PI (5 μg/ml) for 30 min. After washing, the coverslips were mounted with Vectashield (Vector Laboratories Inc., Burlingame, CA, USA) and analysed with a confocal microscope (Radiance 2100 Biorad) at x400 magnification.

Real-time quantitative PCR. RNA was isolated according to RNAwiz protocol (Ambion, USA). Contaminating DNA was removed according to the DNA-free kit (Ambion) and mRNA underwent reverse transcription reaction according to Retroscript protocol (Ambion). Primers (Primm, Italy) and probes (Eurogentec, Belgium) were synthesized for the following sequences: 18S, Cox-1, Cox-2. The sequences were 18S-F, GCCGCTAGAGGTGAAATTCT; 18S-R, CTTGGCAAATGCTTTCGCTC; 18S-P, CCGGCGCAAGACGGACCAGAGCCGG; Cox-2-F, TTACAATGCTGACTATGGCTACAA; Cox-2-R, CTTTGACACCCAAGGGAG; Cox-2-P, CCTCCTGTGCCTGATGATTGCCCGACAGGAGG.

Real-time quantitative RT-PCR was performed with the Taqman system (Biorad) using cDNA from 25 ng of total RNA (31). Fifty cycles were performed using the Platinum Quantitative PCR SuperMix-UDG (Life Technologies), primers for 18S were used at a final concentration of 80 nM, while primers for Cox-1 and Cox-2 were used at a final concentration of 900 nM. Probes were used at a final concentration of 200 nM. Each sample was tested twice. For quantification, the target sequence was normalised in relation to the 18S content.

Transcription assay. Transfection experiments were first performed using HUVECs and EAhy 926 cells. However, the efficiencies reached were very low with a high degree of cytotoxicity (data not shown). As human Cox-2 promoter regulation is similar in a wide number of cell types (34-37), we performed transfection experiments in CHO cells, a cell line widely used for studies involving the effects of HDL *in vitro* (38-41). The construction of various reporter vectors for the human Cox-2 gene has been described previously (26,27). The 5' flanking region (-327 to +59) of the human Cox-2 is co-operatively regulated through 3 *cis*-activating elements, the NF-κB site (-223 to -214), the NF-IL6 site (-132 to -124) and the CRE site (-59 to -52) (26,27). CHO cells were transient transfected with Cox-2 (nucleotide -327/+59), the NF-κB mutated site (KBM), the CRE mutated site (CRM), the NF-IL6 mutated site (ILM) or the (-52/+59) luciferase reporter using lipofectamine (Invitrogen) according to the manufacturer's instructions. Luciferase activity was determined and normalised with the protein concentration (27).

Detection of prostaglandin release by ACE™ competitive enzyme immunoassay. These assays are based on the competition between each prostaglandin (6-keto $PGF_{1\alpha}$, TXB_2 or PGE_2) and each prostaglandin-acetylcholinestarase (AChE) conjugate (6-keto $PGF_{1\alpha}$-AChE, TXB_2-AChE or PGE_2-AchE) for limited specific anti-serum binding sites. The kits were purchased from Cayman (USA). HUVECs were exposed to n-LDL or Ox-LDL (30 μg/ml) for 6 h, washed twice with PBS and then incubated for 30 min with exogenous AA (10 μM). The supernatants were collected, centrifuged at 800 rpm for 10 min and transferred to new tubes. Each

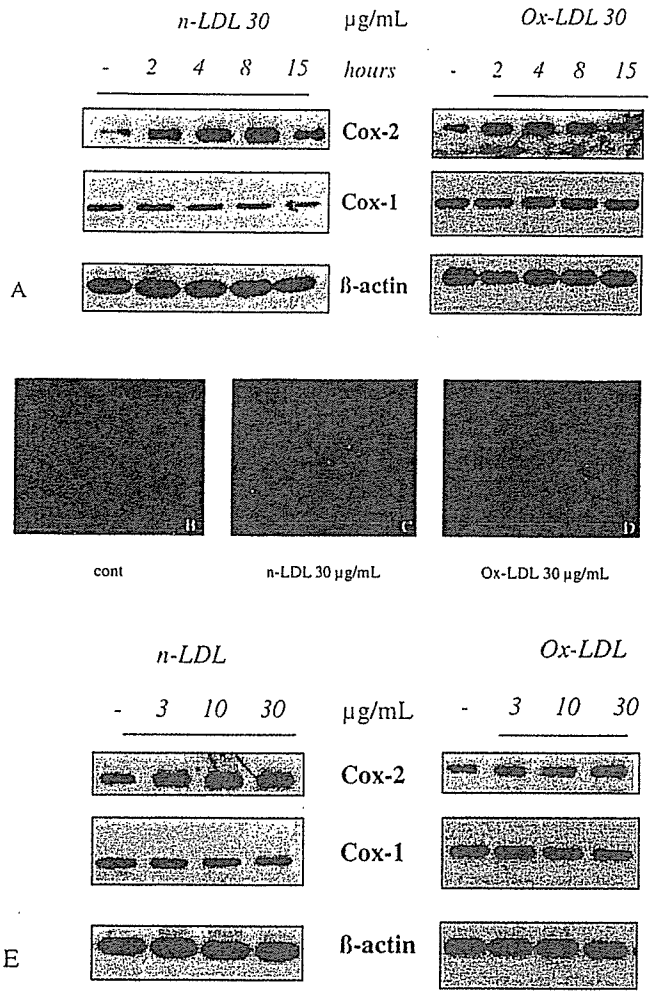

Figure 1. Time- and concentration-dependent effect of native LDL and oxidized LDL on Cox-1 and Cox-2 protein expression. (A), Sparse cultures of HUVEC were incubated for 2-15 h with n-LDL or Ox-LDL (30 µg/ml). The panel refers to a representative experiment. (B), Immunocytochemistry analysis of Cox-2 protein expression (the green signal represents Cox-2 while the red one is the staining with propidium iodide) in control cells or incubated with 30 µg/ml of n-LDL or Ox-LDL (C and D respectively). (E), Sparse cultures of HUVEC were incubated for 4 h with n-LDL or Ox-LDL (3-30 µg/ml). For experiment details see Materials and methods.

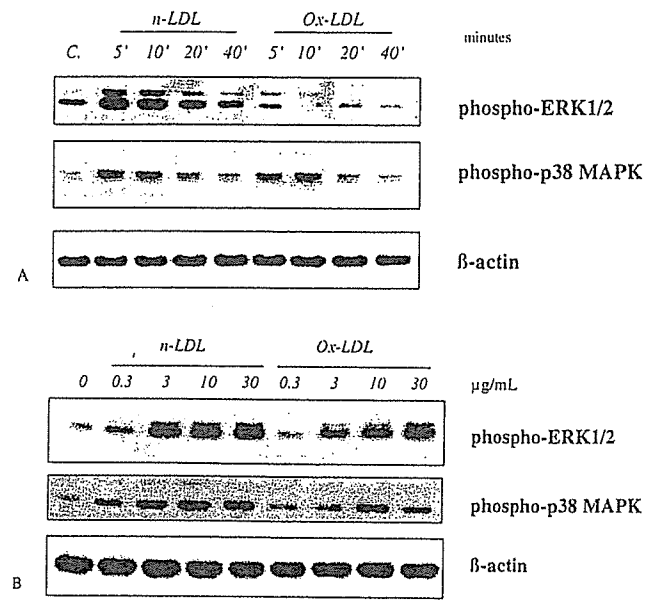

Figure 2. (A), Time dependency of MAPK phosphorylation by native or oxidized LDL. HUVEC were incubated for 5-40 min with n-LDL or Ox-LDL (30 µg/ml). Cell proteins were subjected to SDS-PAGE electrophoresis and immunoblotting with mouse monoclonal phospho-p44/42 MAPK antibody, rabbit polyclonal phospho-p38 MAPK antibody and mouse monoclonal anti-ß-actin antibody. The upper panel refers to a representative experiment. The lower panel depicts the result of 4 different experiments (mean ± SD). *p<0.01 versus relative control values. For experimental details see Materials and methods. (B), Concentration dependency of MAPK phosphorylation by native or oxidized LDL. HUVEC were incubated for 5 min with n-LDL or Ox-LDL (0.3-30 µg/ml). The upper panel refers to a representative experiment. The lower panel depicts the result of 4 different experiments (mean ± SD). *p<0.01 versus relative control values. For experiment details see Materials and methods.

sample (50 µl) was processed for evaluation of prostaglandin release according to the manufacturer's instructions.

Statistical analysis. Data presented in the text and figures are mean ± SD and are representative of 4 different experiments. Statistical analysis was performed by ANOVA with the use of Statsoft Statistica Package.

Results

N-LDL and Ox-LDL induce Cox-2 expression in HUVECs. Cox-2 protein was expressed at low levels in unstimulated cells and was strongly induced 2 h after exposure to n-LDL or Ox-LDL (30 µg/ml), the induction was maximal after 4 h, sustained up to 8 h and decreased after 15 h (Fig. 1) (Cox-2 expression in unstimulated cells remained low at all time points, data not shown). Neither n-LDL nor Ox-LDL affected Cox-1 expression (Fig. 1). N-LDL and Ox-LDL induced Cox-2 protein expression in a dose-dependent manner (from 3-30 µg/ml) (Fig. 1). These findings were confirmed with immunocytochemistry, an increase of Cox-2 expression was detected after 4 h in cells incubated with n-LDL and Ox-LDL (Fig. 1).

N-LDL and Ox-LDL activate p44/p42 (ERK1/2) MAPK and p38 MAPK. Since Cox-2 expression is regulated through a MAPK-dependent pathway in macrophages, smooth muscle cells or endothelial cells (19-23), we investigated the ability of n-LDL and Ox-LDL to activate ERK1/2 and/or p38 MAPK in HUVEC. It has been established that ERK1/2 are activated when ^{202}Thr and ^{204}Tyr are both phosphorylated (42), and that p38 MAPK is activated when ^{180}Thr and ^{182}Tyr are both phosphorylated (43). The phosphorylation of ERK1/2 and p38 MAPK has been widely used as an indicator of its activation (42,43). In a preliminary time course experiment with endothelial cells, the peak of activity of n-LDL or Ox-LDL was reached 5 and 10 min after stimulation (Fig. 2A), similar to previously reported data in smooth muscle cells and in macrophages (42,43). Therefore in all following experiments, cells were pre-incubated with serum-free medium for at least 6 h and then n-LDL or Ox-LDL were added for 5 min. Our data demonstrate that n-LDL in human endothelial cells activates ERK1/2 and p38 MAPK in a concentration-dependent manner (Fig. 2B). Ox-LDL induces phosphorylation of p38 MAPK to a large extent, while ERK1/2 phosphorylation is

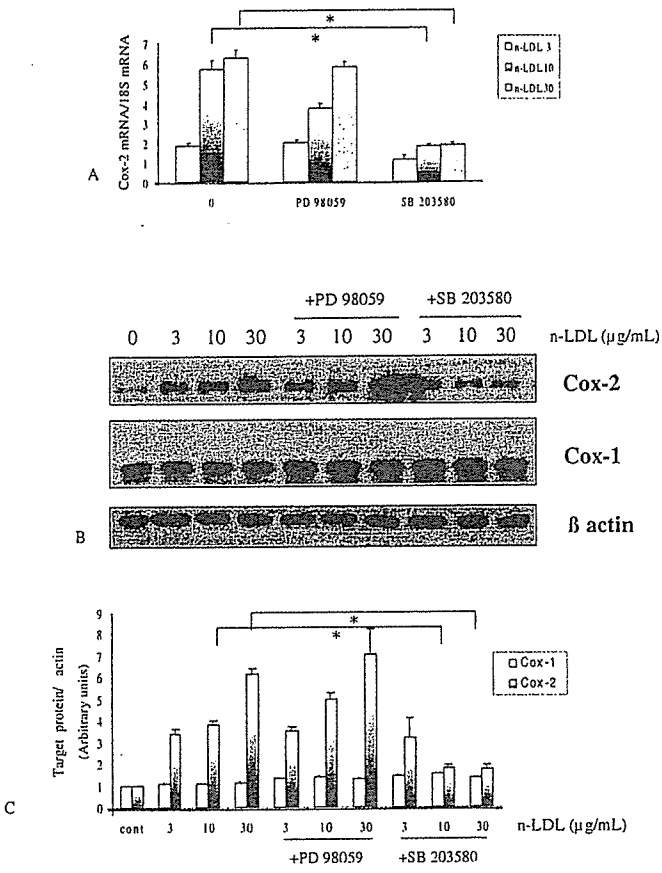

Figure 3. Involvement of p38 MAPK pathway in Cox-2 mRNA and protein expression induced by native LDL. HUVEC were incubated for 2 and 4 h with n-LDL (3-30 µg/ml) alone or in the presence of the MEK1 inhibitor, PD98059 (25 µM) or of the p38 MAPK inhibitor SB203580 (0.5 µM). (A), The Cox-2 mRNA expression was assessed with the real-time quantitative PCR. For quantification the target sequence was normalized in relation to the 18S content. (B), Cell proteins were subjected to SDS-PAGE electrophoresis and immunoblotting with anti-Cox-2, anti-Cox-1 and anti-ß-actin antibodies. The panel refers to a representative experiment. (C), The panel depicts the result of 6 different experiments (mean ± SD). *p<0.01 versus relative control values. For experiment details see Materials and methods.

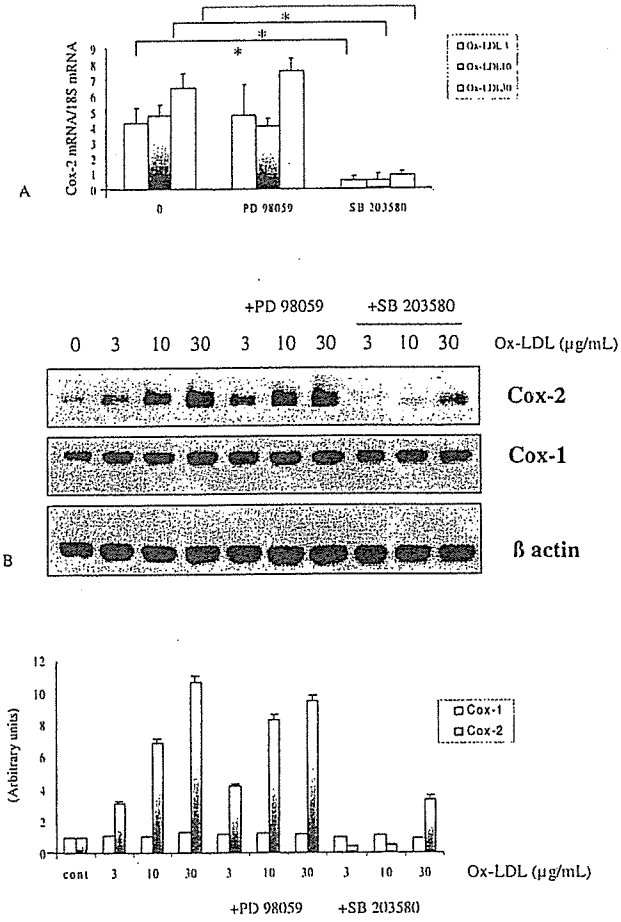

Figure 4. Involvement of p38 MAPK pathway in Cox-2 mRNA and protein expression induced by Ox-LDL. HUVEC were incubated for 2 and 4 h with Ox-LDL (3-30 µg/ml) alone or in the presence of the MEK1 inhibitor, PD98059 (25 µM) or of the p38 MAPK inhibitor SB203580 (0.5 µM). (A), The Cox-2 mRNA expression was assessed with the real-time quantitative PCR. For quantification, the target sequence was normalized in relation to the 18S content. (B), Cell proteins were subjected to SDS-PAGE electrophoresis and immunoblotting with anti-Cox-2, anti-Cox-1 and anti-ß-actin antibodies. The panel refers to a representative experiment. (C), The panel depicts the result of 6 different experiments (mean ± SD). *p<0.01 versus relative control values. For experiment details see Materials and methods.

lower if compared with n-LDL-induced phosphorylation. An increase of MAPKs activity was detected at n-LDL or Ox-LDL concentration as low as 3 µg/ml. Therefore, in all experiments cells were incubated with Ox-LDL concentrations ranging from 3-30 µg/ml as the half-maximal response with Ox-LDL at 15 µg/ml for ERK1/2, and 20 µg/ml for p38 MAPK in smooth muscle cells and macrophages, respectively (42,43).

Involvement of MAPK in n-LDL- and Ox-LDL- induced Cox-2 protein and mRNA expression. To investigate the role of ERK1/2 and p38 MAPK pathways in Cox-2 expression induced by n-LDL or Ox-LDL, cells were pre-incubated with the MEK1 inhibitor PD 98059 (25 µM) or the p38 MAPK inhibitor SB 203580 (0.5 µM) for 1 h. N-LDL or Ox-LDL (3-30 µg/ml) were then added for 2 and 4 h to evaluate Cox-2 and Cox-1 mRNA and protein expression (Fig. 3 and 4). PD 98059 was unable to block n-LDL or Ox-LDL induced Cox-2 expression or to alter Cox-1 expression. SB 203580 strongly inhibited n-LDL or Ox-LDL-induced Cox-2 expression. No effect was observed on Cox-1 expression.

Effects of n-LDL and Ox-LDL on Cox-2 promoter activity. Next we examined the effects of n-LDL and Ox-LDL on the Cox-2 promoter activity. The human Cox-2 promoter region (-327/+59) contains the NF-κB, the NF-IL6 and the CRE sites (26,27). Transient transfection assay showed that n-LDL induced promoter activity by 2.96±0.03-fold, while Ox-LDL induced promoter activity by 4.24±0.029-fold (Fig. 5). The promoter activity of the construct carrying the mutation at the NF-κB site was inhibited by 47% with n-LDL and by 52% with Ox-LDL. The promoter activity of the construct carrying the mutation at the NF-IL6 site was inhibited by 41% with n-LDL and by 43% with Ox-LDL, and that of the construct carrying the mutation at the CRE site was inhibited by 56% with n-LDL and by 39% with Ox-LDL (Fig. 5).

Effects of n-LDL and Ox-LDL on prostaglandin release. The effects of n-LDL and Ox-LDL on prostaglandin production were assessed in HUVECs exposed to 30 µg/ml of lipoproteins. Because PGI_2 and TXA_2 main metabolites are unstable, 6-keto

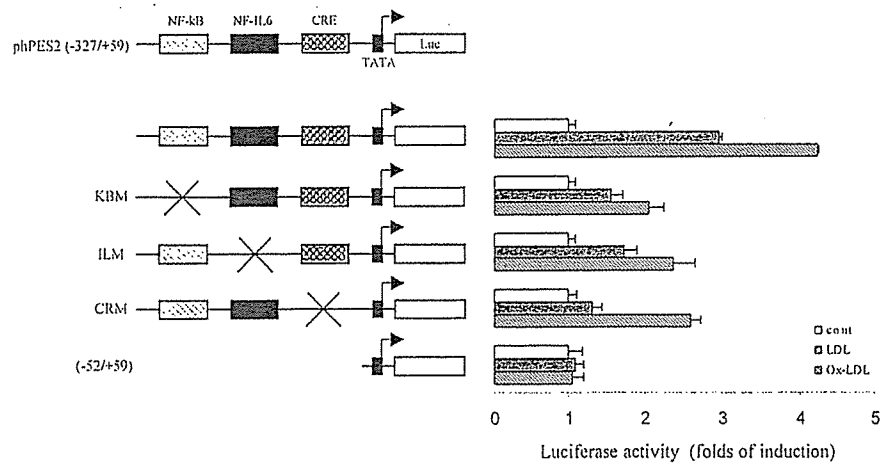

Figure 5. Identification of the regions responsible for n-LDL and Ox-LDL induced promoter activity of the human Cox-2 gene. The 5'-flanking region of the human Cox-2 gene with site specific mutations are represented schematically on the left. Following transfection, CHO cells were incubated for 6 h with n-LDL or Ox-LDL (30 μg/ml). The results are presented as relative luciferase activity normalized to cellular protein content. Each experiment was carried out in triplicate. For experiment details see Materials and methods.

$PGF_{1\alpha}$ and TXB_2 were measured in the cell supernatant using the ACE™ competitive enzyme immunoassay. The same assay was used to measure PGE_2 release. High amounts of 6-keto $PGF_{1\alpha}$ (67.28±4.22 pg/ml) and of PGE_2 (46.86± 1.40 pg/ml) are produced under basal conditions. Neither n-LDL nor Ox-LDL modified 6-keto $PGF_{1\alpha}$ (64.91±4.84 and 70.96±1.74 pg/ml). PGE_2 release was significantly increased by n-LDL (68.31±1.95 pg/ml) and by Ox-LDL (64.19±3.06 pg/ml) ($p<0.01$ versus relative control values). This effect was reverted in part (53.4±2.7 pg/ml for n-LDL and 56.2±1.8 pg/ml for Ox-LDL) when cells were incubated in the presence of 0.1 μM indomethacin eptyl ester, (the modification of indomethacin to an eptyl ester derivate generates a molecule that selectively inhibits Cox-2 (32)). TXB_2 release was low under basal conditions (2.34±0.14 pg/ml) and was not affected by n-LDL or Ox-LDL incubation.

Discussion

The major finding of the present study is that both n-LDL and Ox-LDL can induce Cox-2 expression and PGE_2 release in HUVEC, an effect that is dependent mainly on p38 MAPK NF-κB CRE-dependent pathways.

N-LDL activated ERK1/2 and p38 MAPK in a concentration-dependent manner (3-30 μg/ml), a concentration 40- to 400-fold lower than that reported by Zhu *et al* (44) to stimulate p38 MAPK. Ox-LDL also induced ERK1/2 phosphorylation although to a lower extent. The rapid onset of the MAPK response in endothelial cells (within 5 min for both ERK1/2 and p38 MAPK) suggests that the activation of the MAPK signalling cascade by n-LDL or Ox-LDL is independent of the internalisation of lipoproteins. A role for the interaction of these lipoproteins with membrane receptors cannot be ruled out if it is assumed that n-LDL, Ox-LDL or some of their constituents, interact with signal-transducing receptors at the plasma membrane level. Preliminary experiments suggest that lipids contained in the polar fractions seem to be responsible for p38 MAPK activation and Cox-2 expression (data not shown).

Several genes have been shown to be regulated through a MAPK-dependent pathway (19-23). Among these, Cox-2 is believed to play a relevant role in inflammatory diseases such as atherosclerosis (2,3,15,16). Our results clearly show that n-LDL and Ox-LDL induce Cox-2 expression in endothelial cells. Previous data showed opposite effects of Ox-LDL in macrophages (45,46). However, *ex-vivo* data suggest a conspicuous staining of Cox-2, colocalizing mainly with macrophages and endothelial cells, in atherosclerotic plaques but not in normal arteries (2,3). In this study we report the finding that n-LDL can induce the expression of Cox-2 in human endothelial cells, although to a lesser extent than that obtained with Ox-LDL. This is not the first evidence of a possible direct pro-atherogenic role of n-LDL. In fact, it has been reported that n-LDL can induce the expression of VCAM-1 and E-selectin in porcine vascular endothelial cells (4), suggesting that endothelial cells can be activated to an inflammatory state following contact with unmodified forms of LDL. Alternatively, one could speculate that minimal oxidation is occurring in our lipoprotein preparations. We took all precautions to avoid unwanted oxidative modifications, furthermore the conjugated diene content was very low and no signs of apo B degradation were detected in SDS gel electrophoresis loading the gel <30 μg of protein (data not shown).

Our findings that p38 MAPK inhibition reduces both the n-LDL- or Ox-LDL-induced Cox-2 expression to a very large extent indicates that this is the major signal transducing pathway responsible for this effect. These findings are in agreement with a major role for this pathway in modulating some of the pro-inflammatory responses induced by n-LDL or Ox-LDL (5). P38 MAPK can regulate Cox-2 expression at both transcriptional and post-transcriptional levels in human monocytes (47). In this work the authors suggest that a basal level of p38 MAPK activity plays a housekeeping role in maintaining Cox-2 mRNA stability while a full induction of p38 MAPK activity is required for induction of Cox-2 transcripts. Transient transfection with the Cox-2 promoter, (-327/+59) wild-type or carrying mutations for the NF-κB, NF-IL6 and CRE sites showed that all these trascription factors potentially regulated via p38 MAPK (48), are involved

in n-LDL or Ox-LDL induced Cox-2 gene trascription. However a role for p38 MAPK in stabilising Cox-2 mRNA in endo-thelial cells can not be excluded (32). Two reports stressed that caution is needed in the use of SB 203580 (49,50) as higher concentrations of SB 203580 (10 μM) could also inhibit JNK. This does not apply in our case as the concentration used (0.5 μM) is the IC50 for p38 MAPK and did not affect the activity of a wide range of protein kinases, including JNKs (48).

The possibility that Cox-2 plays a harmful role by catalysing the biosynthesis of pro-inflammatory prostanoids has been suggested (28). Baker *et al* (3) demonstrated Cox-2 immunostaining in macrophages/foam cells, intimal and medial smooth muscle cells and endothelial cells in atherosclerotic arteries, whereas normal arteries contained no Cox-2 protein. Similarly, Schonbeck *et al* (2) found expression of both Cox-1 and Cox-2 by endothelial cells, smooth muscle cells and macrophages in atherosclerotic arteries, while normal arteries only expressed Cox-1. Furthermore, Cox-2 and prostaglandin synthase E colocalize in symptomatic lesions and are possibly involved in metalloprotease activation via PGE_2 production (51), suggesting a role for PGE_2 in plaques instability. Our data fit with this hypothesis, as PGE_2 was the main product of Cox-2 induced by n-LDL and Ox-LDL. To this respect Cox-2 induction and PGE_2 release by n-LDL and Ox-LDL could explain, at least in part, the relation observed between the levels of Ox-LDL in the plaques and plaque instability (52).

On the other hand, Cox-2 might play an atheroprotective role (53,54). *In vitro* laminar shear stress upregulates Cox-2 mRNA and protein in HUVEC, turbulent shear stress does not have this effect (53). Similarly lysophosphatidylcholine-induced the expression of Cox-2 in HUVEC and subsequent enhancement of endothelial synthesis of prostacyclin (54). Prostacyclin is a potent vasodilator, inhibits platelet aggregation and blocks leukocyte adhesion and activation (55,56). It is therefore possible that Cox-2 induced in endothelial cells at lesion-protected areas catalyses the formation of the anti-atherogenic molecule prostacyclin. However, this is not our case as no increase in prostacyclin synthesis was observed. Furthermore, Cox-2 expression induced by HDL has been involved in prostacyclin synthesis (32,57). These findings suggest the possibility that Cox-2 induction alone is not enough to drive prostaglandin production toward a pro-atherogenic or anti-atherogenic profile, but it is the prostanoid produced that accounts for this effect.

In summary we have shown that n-LDL and Ox-LDL induce Cox-2 expression in human endothelial cells through a p38 MAPK, NF-κB, CRE dependent pathway. This is followed by n-LDL and Ox-LDL induced PGE_2 release, which has recently been associated with plaque instability (51), suggesting a new mechanism by which cholesterol rich lipoproteins could affect the arterial wall.

Acknowledgements

This study was supported by a grant from CIRC (Consorzio Interuniversitario Ricerca Cardiovascolare) and FIRST 2002 to ALC, and a grant from MIUR (Ministero Università e Ricerca Scientifica) to GDN. The authors are grateful to Roberto Zecca and Giulio Simonutti for technical assistance.

References

1. Campbell WB and Halushka PV: Lipid-derived autacoids: eicosanoids and platelet-activating factor. In: The Pharmacological Basis of Therapeutics. Hardman JG and Limbird LE (eds). 9th edition. McGraw-Hill, New York, pp601-616, 1996.
2. Schonbeck U, Sukhova GK, Graber P, Coulter S and Libby P: Augmented expression of cyclooxygenase-2 in human atherosclerotic lesions. Am J Pathol 155: 1281-1291, 1999.
3. Baker CS, Hall RJ, Evans TJ, Pomerance A, Maclouf J, Cremionon C, Yacoub MH and Polak JM: Cyclooxygenase-2 is widely expressed in atherosclerotic lesions affecting native and transplanted human coronary arteries and colocalizes with inducible nitric oxide synthase and nitrotyrosine particularly in macrophages. Arterioscler Thromb Vasc Biol 19: 646-655, 1999.
4. Ross R: Atherosclerosis - an inflammatory disease. N Engl J Med 340: 115-126, 1999.
5. Allen S, Khan S, Al-Mohanna F, Batten P and Yacoub M: Native low density lipoprotein-induced calcium triggers VCAM-1 and E-selectin expression in cultured human vascular endothelial cells. J Clin Invest 101: 1064-1075, 1998.
6. Witzum JL and Steinberg D: Role of oxidized low density lipoprotein in atherogenesis. J Clin Invest 88: 1785-1792, 1991.
7. Parhami F, Fang ZT, Fogelman AM, Andalibi A, Territo MC and Berliner JA: Minimally modified low density lipoprotein-induced inflammatory response in endothelial cells are mediated by cyclic adenosine monophosphate. J Clin Invest 92: 471-478, 1993.
8. Smalley DM, Lin JH, Curtis ML, Kobari Y, Stemerman MB and Prichard KAJ: Native LDL increases endothelial cell adhesiveness by inducing intercellular adhesion molecule-1. Arterioscler Thromb Vasc Biol 16: 585-590, 1996.
9. Pirillo A, Norata GD, Zanelli T and Catapano AL: Overexpression of HSP70i in COS-1 cells fails to protect from the cytotoxicity of Ox-LDL. Arterioscler Thromb Vasc Biol 21: 348-354, 2001.
10. Norata GD, Tonti L, Roma P and Catapano AL: Apoptosis and proliferation of endothelial cells in early atherosclerotic lesions: a possible role for oxidized LDL. Nutr Met Cardiovasc Dis 12: 297-305, 2002.
11. Pirillo A, Zhu W, Norata GD, Zanelli T, Barberi L, Roma P and Catapano AL: Oxidized lipoproteins and endothelium. Clin Chem Lab Med 38: 155-160, 2000.
12. Norata GD, Bjork H, Hamsten A, Catapano AL and Eriksson P: High density lipoprotein decrease ADAMTs1 expression induced by LPS and TNFα in human endothelial cells. Matrix Biol (In press).
13. Fyrnys B, Claus R, Wolf G and Deigner HP: Oxidized low density lipoprotein stimulates protein kinase C (PKC) activity and expression of PKC-isotypes via prostaglandin-H-synthase in P388D1 cells. Adv Exp Med Biol 407: 93-98, 1997.
14. Larrue J, Rigaud M, Daret D, Demond J, Durand J and Bricaud H: Prostacyclin production by cultured smooth muscle cells from atherosclerotic rabbit aorta. Nature 285: 480-482, 1980
15. Moncada S: Prostacyclin and arterial wall biology. Arteriosclerosis 2: 193-207, 1982
16. Willis AL, Smith DL and Vigo C: Suppression of principal atherosclerotic mechanism by prostacyclins and other eicosanoids. Prog Lipid Res 25: 645-666, 1986.
17. Vane JR, Bakhle Y and Botting R: Cyclooxygenase-1 and -2. Annu Rev Pharmacol Toxicol 38: 97-120, 1998.
18. DuBois RN, Abramson SB, Crofford L, Gupta RA, Simon LS, Van De Putte LBA and Lipsy PE: Cyclooxygenase in biology and disease. FASEB J 12: 1063-1073, 1998.
19. Bartlett SR, Sawdy R and Mann GE: Induction of cyclooxygenase-2 expression in human myometrial smooth muscle cells by interleukin-1 beta: involvement of p38 mitogen-activated protein kinase. J Physiol 520: 399-406, 1999.
20. Lee SH, Soyoola E, Chanmugam P, Hart S, Sun W, Zhong H, Liou S, Simmons D and Hwang D: Selective expression of mitogen-inducible cyclooxygenase in macrophages stimulated with lipopolysaccharide. J Biol Chem 267: 25934-25938, 1992.
21. Bornfeldt KE, Campbell JS, Koyama H, Argast GM, Leslie CC, Raines EW, Krebs EG and Ross R: The mitogen-activated protein kinase pathway can mediate growth inhibition and proliferation in smooth muscle cells: dependence on the availability of downstream targets. J Clin Invest 100: 875-885, 1997.
22. Guan Z, Buckman SY, Miller BW, Springer LD and Morrison AR: Interleukin-1ß-induced cyclooxygenase-2 expression requires activation of both c-Jun NH2-terminal kinase and p38 MAPK signal pathway in rat mesangial cells. J Biol Chem 273: 28670-28676, 1998.

23. LaPointe MC and Isenovic E: Interleukin-1ß regulation of inducible nitric oxide synthase and cyclooxygenase-2 involves the p44/44 and p38 MAPK signaling pathways in cardiac myocytes. Hypertension 33 (suppl II): 276-282, 1999.
24. Seger R and Krebs EG: The MAPK signaling cascade. FASEB J 9: 726-735, 1995.
25. Hazzalin CA and Mahadevan LC: MAPK-regulated transcription: a continuously variable gene switch? Nat Rev Mol Cell Biol 3: 30-40, 2002
26. Inoue H, Yokoyama C, Hara S, Tone Y and Tanabe T: Transcriptional regulation of human prostaglandin-endoperoxide synthase-2 gene by lipopolysaccharide and phorbol ester in vascular endothelial cells. Involvement of both nuclear factor for interleukin-6 expression site and cAMP response element. J Biol Chem 270: 24965-24971, 1995.
27. Inoue H, Umesono K, Nishimori T, Hirata Y and Tanabe T: Glucocorticoid-mediated suppression of the promoter activity on the cyclooxygenase-2 gene is modulated by expression of its receptor in vascular endothelial cells. Biochem Biophys Res Comm 254: 292-298, 1999.
28. Linton MF and Fazio S: Cyclooxygenase-2 and atherosclerosis. Curr Opin Lipidol 13: 497-504, 2002.
29. Havel RJ, Eder HA and Bragdon JH: The distribution and chemical composition of ultracentrifugally separated lipoprotein in human serum. J Clin Invest 34: 1345-1353, 1955.
30. Lowry OH, Rosebrough HJ, Farr AR and Randall RJ: Protein measurement with the Folin-phenol reagent. J Biol Chem 193: 265-275, 1951.
31. Norata GD, Pellegatta F, Hamsten A, Catapano AL and Eriksson P: Effects of high density lipoprotein subfraction 3 on the expression of matrix-degrading proteases in human endothelial cells. Int J Mol Med 12: 73-78, 2003
32. Norata GD, Callegari E, Inoue H and Catapano AL: High density lipoproteins induce cyclooxygenase-2 expression and prostacyclin synthesis in human endothelial cells via a p38 MAPK/CRE dependent pathway. Effects on COX-2/PGI-S coupling. Arterioscler Thromb Vasc Biol (In press).
33. Norata GD, Pirillo A, Callegari E, Hamsten A, Catapano AL and Eriksson P: Gene expression analysis of human endothelial cells incubated with VLDL and Ox-VLDL. Cardiovasc Res 59: 169-180, 2003.
34. Singer CA, Baker KJ, McCaffrey A, AuCoin DP, Dechert MA and Gerthoffer WT: P38 MAPK and NF-{kappa}B mediate COX-2 expression in human airway myocytes. Am J Physiol Lung Cell Mol Physiol 285: L1087-L1098, 2003.
35. Loudon JA, Elliott CL, Hills F and Bennett PR: Progesterone represses interleukin-8 and cyclooxygenase-2 in human lower segment fibroblast cells and amnion epithelial cells. Biol Reprod 69: 331-337, 2003.
36. Tamura M, Sebastian S, Yang S, Gurates B, Fang Z, Okamura K and Bulun SE: Induction of cyclooxygenase-2 in human endometrial stromal cells by malignant endometrial epithelial cells: evidence for the involvement of extracellularly regulated kinases and CCAAT/enhancer binding proteins. J Mol Endocrinol 31: 95-104, 2003.
37. Kaltschmidt B, Linker RA, Deng J and Kaltschmidt C: Cyclooxygenase-2 is a neuronal target gene of NF-kappaB. BMC Mol Biol 3: 16, 2002.
38. Baez JM, Barbour SE and Cohen DE: Phosphatidylcholine transfer protein promotes apolipoprotein A-I-mediated lipid efflux in Chinese hamster ovary cells. J Biol Chem 277: 6198-6206, 2002.
39. Ioka RX, Kang MJ, Kamiyama S, Kim DH, Magoori K, Kamataki A, Ito Y, Takei YA, Sasaki M, Suzuki T, Sasano H, Takahashi S, Sakai J, Fujino T and Yamamoto TT: Expression cloning and characterization of a novel glycosylphosphatidylinositol-anchored high density lipoprotein-binding protein, GPI-HBP1. J Biol Chem 278: 7344-7349, 2003.
40. Fuki IV, Blanchard N, Jin W, Marchadier DH, Millar JS, Glick JM and Rader DJ: Endogenously produced endothelial lipase enhances binding and cellular processing of plasma lipoproteins via heparan sulfate proteoglycan-mediated pathway. J Biol Chem 278: 34331-34338, 2003.
41. Witting SR, Maiorano JN and Davidson WS: Ceramide enhances cholesterol efflux to apolipoprotein A-I by increasing the cell surface presence of ATP-binding cassette transporter A1. J Biol Chem 278: 40121-40127, 2003.
42. Kusuhara M, Chait A, Cader A and Berk BC: Oxidized LDL stimulates mitogen-activated protein kinase in smooth muscle cells and macrophages. Arterioscler Thromb Vasc Biol 17: 141-148, 1997.
43. Jing Q, Xin SM, Cheng ZJ, Zhang WB, Zhang R, Qin YW and Pei G: Activation of p38 mitogen-activated protein kinase by oxidized LDL in vascular smooth muscle cells. Circ Res 84: 831-839, 1999.
44. Zhu YI, Liao H, Wang N, Ma KS, Verna LK, Shyy JYJ, Chien S and Stemerman MB: LDL-activated p38 in endothelial cells is mediated by ras. Arterioscler Thromb Vasc Biol 21: 1159-1164, 2001.
45. Eligini S, Colli S, Basso F, Sironi L and Tremoli E: Oxidized low density lipoprotein suppresses expression of inducible cyclooxygenase in human macrophages. Arterioscler Thromb Vasc Biol 19: 1719-1725, 1999.
46. Pontsler AV, St Hilaire A, Marathe GK, Zimmerman GA and McIntyre TM: Cyclooxygenase-2 is induced in monocytes by peroxisome proliferator activated receptor gamma and oxidized alkyl phospholipids from oxidized low density lipoprotein. J Biol Chem 277: 13029-13036, 2002.
47. Dean JLE, Brook M, Clark AR and Saklatvala J: P38 MAPK regulates cyclooxygenase-2 mRNA stability and transcription in lipopolysaccharide-treated human monocytes. J Biol Chem 274: 264-269, 1999.
48. Guha M and Mackman N: LPS induction of gene expression in human monocytes. Cell Signal 13: 85-94, 2001.
49. Clerk A and Sugden PH: The p38-MAPK inhibitor, SB203580, inhibits cardiac stress-activated protein kinases/c-Jun N-terminal kinases (SAPKs/JNKs). FEBS Lett 426: 93-96, 1998.
50. Whitmarsh AJ, Yang SH, Su MS, Sharrocks AD and Davis RJ: Role of p38 and JNK mitogen-activated protein kinases in the activation of ternary complex factors. Mol Cell Biol 17: 2360-2371, 1997.
51. Cipollone F, Prontera C, Pini B, Marini M, Fazia M, De Cesare D, Iezzi A, Ucchino S, Boccoli G, Saba V, Chiarelli F, Cuccurullo F and Mezzetti A: Overexpression of functionally coupled cyclooxygenase-2 and prostaglandin E synthase in symptomatic atherosclerotic plaques as a basis of prostaglandin E(2)-dependent plaque instability. Circulation 104: 921-927, 2001.
52. Nishi K, Itabe H, Uno M, Kitazato KT, Horiguchi H, Shinno K and Nagahiro S: Oxidized LDL in carotid plaques and plasma associates with plaque instability. Arterioscler Thromb Vasc Biol 22: 1649-1654, 2002.
53. Topper JN, Cai J, Falb D and Gimbrone MAJ: Identification of vascular endothelial genes differentially responsive to fluid mechanical stimuli: cyclooxygenase-2, manganese superoxide dismutase, and endothelial cell nitric oxide synthase are selectively up-regulated by steady laminar shear stress. Proc Natl Acad Sci USA 93: 10417-10422, 1996.
54. Zembowicz A, Jones SL and Wu KK: Induction of cyclooxygenase-2 in human umbilical vein endothelial cells by lysophosphatidylcholine. J Clin Invest 96: 1688-1692, 1995.
55. Wu KK: Cyclooxygenase-2 induction: molecular mechanism and pathophysiologic roles. J Lab Clin Med 128: 242-245, 1996.
56. Vane JR and Botting RM: Pharmacodynamic profile of prostacyclin. Am J Cardiol 75: 3A-10A, 1995.
57. Vinals M, Martinez-Gonzalez J and Badimon L: Regulatory effects of HDL on smooth muscle cell prostacyclin release. Arterioscler Thromb Vasc Biol 19: 2405-2411, 1999.

Transmission of Force and Displacement within the Myosin Molecule†

Takashi Ohki,‡ Sergey V. Mikhailenko,‡ Manuel F. Morales,§ Hirofumi Onishi,*,‡ and Naoki Mochizuki‡

Department of Structural Analysis, National Cardiovascular Center Research Institute, Fujishiro-dai, Suita, Osaka 565-8565, Japan, and University of the Pacific, San Francisco, California 94115

Received May 23, 2004; Revised Manuscript Received August 14, 2004

ABSTRACT: Myosin is a repetitive impeller of actin, using its catalysis of ATP hydrolysis to derive repeatedly the required free energy decrements. In each impulsion, changes at the myosin active site are transmitted through a series of structural elements to the myosin propeller (lever arm), almost 5 nm away. While the nature of transmission through most elements is evident, that through the so-called converter is not. To investigate how the converter changes linear displacement into rotation, we tested (one at a time) the effect of two Phe residue mutations (at 721 and 775) in the converter on the overall function of a heavy meromyosin (or subfragment 1) system, after first showing by observing kinetic behaviors that neither mutation affects other elements in the transmission. Using three tests (direct movement of the lever arm, activity in a motility assay with actin filaments, and direct force measurement of lever arm function), we found that these mutations affected only movements of the converter and the lever arm. From interpreting our observations in terms of the structure of the converter, we deduce that the linear−rotational transformation in the converter is mediated by a little machine (two Phe residues linked to a Gly) within a machine.

Myosin is the enzyme that catalyzes the hydrolysis of ATP, liberating the free energy used for the actin-propelling work in muscle contraction (*1*, *2*). But now, at the scale that can be accessed by X-ray crystallography and electron microscopy, myosin is seen as a complicated machine of many moving parts (*3*−*9*). Its catalytic function (conducted at its active site) is a long distance from the site of its actin propeller (lever arm) (*5*, *6*). Intervening are the relay helix and a poorly understood structure called the converter (*7*, *8*). When hydrolysis at the active site is transduced into force and displacement, these effects are transmitted by the intervening elements to the lever arm (*7*, *8*). Our aim is to understand how the overall transmission is accomplished, so we have to determine how the converter works. To get at this, we alter the converter structure by two especially chosen site-directed mutations, and draw inferences from what we observe. However, what we observe (changes in the movement of the lever arm resulting from a mutation) is meaningful only if we are sure that the mutation alters the converter element alone. Logically, we must begin with evidence that this is true.

The chemical kinetics describing the changes undergone by a myosin system are aptly described by the differential equation of Bagshaw and Trentham (B−T) (*10*, *11*). The equation tracks in time, t, the linear succession of the predominant myosin species, $M_i(t)$, as the enzyme binds the substrate and changes conformation, etc., and later as it sheds first the inorganic phosphate (P_i) and then ADP. Elsewhere, we (*12*, *13*) and others (*14*, *15*) show why the early stages in this succession report transformations at, or near, the active site, and then remote effects on the relay helix. Toward the end of ATP degradation, the stages report the $M_i(t)$ during the release of products, P_i and ADP. Once the numerical values of the rate constants of the equation are known, the equation allows the complete simulation of the degradation, or, if one wishes, of its early and late phases.

With this prospect in mind, three heavy meromyosin (HMM)[1] systems are prepared. One is normal (wild-type) HMM, and the others are the special mutants, in which Phe residues at positions 721 and 775 are replaced with Ala (F721A and F775A, respectively). It is known that both altered positions are located within the converter (*7*). With each system, standard experiments are performed to obtain the matrix of B−T rate constants, wherein some constants alone describe the early and some the late stages of ATP degradation. By comparing the kinetic data from the wild-type and mutant systems, we find that these particular mutations do not matter in the early events involving the active site or the relay helix, and also that they do not matter in the late events of ATP degradation. These findings warrant the conclusion that when performance tests of transmission detect any differences upon mutation, the differences are, most likely, effects on the converter, not adventitious effects on other elements of the system. Next, using three performance tests of transmission, we show that the test scores

† Supported by grants from the Ministry of Education, Culture, Sports, Science and Technology (to H.O. and N.M.), from the Ministry of Health, Labour and Welfare (to N.M.), and from the National Science Foundation (to M.F.M.).

* To whom correspondence should be addressed. Telephone: +81-6-6833-5012. Fax: +81-6-6872-8092. E-mail: honishi@ri.ncvc.go.jp.

‡ National Cardiovascular Center Research Institute.

§ University of the Pacific.

[1] Abbreviations: HMM, heavy meromyosin; S1, subfragment 1; mant-ATP, 2′(3′)-*O*-(*N*-methylanthraniloyl)adenosine 5′-triphosphate; RLC, regulatory light chain; ELC, essential light chain; CFP, cyan fluorescent protein; YFP, yellow fluorescent protein.

10.1021/bi048954f CCC: $27.50
Published on Web 10/09/2004

differ greatly in the middle phase involving the converter. After understanding the detailed structure of the converter, we work back by model building to understand how nucleotide binding, cleft closure, and subsequent events are connected with the converter, and thus, we obtain an overview of the transmission process (in the Discussion).

MATERIALS AND METHODS

Preparation of Recombinant HMMs and S1s. A chicken smooth-muscle myosin heavy chain cDNA clone was supplied by T. Masaki (*16*). A baculovirus transfer vector for wild-type HMM, with the His tag sequence at its N-terminal end and the myc tag sequence at its C-terminal end, in pFastBacHTa (Clontech, Palo Alto, CA), was produced as described previously (*17*). Site-directed mutagenesis was carried out using Kunkel's method (*18*) to replace Phe-721 or Phe-775 in the heavy chain sequence with alanine residues.

The cDNA for yellow fluorescent protein (YFP) was amplified from pEYFP-C1 (Clontech, Palo Alto, CA) by the polymerase chain reaction (PCR), creating an *Afl*III site at its N-terminus and an *Nco*I site at its C-terminus. The PCR product was digested with *Afl*III and *Nco*I, and subcloned into pFastBacHTa (named pFastBacHT-YFP). A transfer vector for the full-length sequence of the YFP-fused subfragment 1 (S1) heavy chain was prepared as described previously (*19*), but with pFastBacHT-YFP instead of pFastBacHTa.

The cDNA for cyan fluorescent protein (CFP) was amplified from pECFP-C1 (Clontech) by PCR with the same primers that were used in amplifying YFP. The PCR product was digested with *Afl*III and *Nco*I, and subcloned into pFastBacNN (*19*) (named pFastBacNN-CFP). pG17-1, which was plasmid pUC118 encoding the myosin essential light chain (ELC) and including a unique *Afl*III site at its initiating methionine codon (*20*), was digested with *Afl*III and *Pst*I, and subcloned into pFastBacNN-CFP. pRLCA, which was plasmid pUC119 encoding the myosin regulatory light chain (RLC) (*20*), was digested with *Afl*III and *Eco*RI, and subcloned into pFastBacNN. A *Bst*1107I site was created at the unique *Avr*II site of the transfer vector and was then digested with *Bst*1107I. To make a transfer vector for both myosin light chains, a cDNA fragment containing the coding region of the RLC was ligated into the *Bst*1107I site of the transfer vector containing the CFP-fused ELC sequence.

Expression and purification of wild-type and mutant HMMs were carried out as described previously (*17*). Chimeric S1s (named C/Y-S1), in which YFP was fused to the N-terminus of the S1 heavy chain and CFP was fused to the N-terminus of the ELC, were prepared by essentially the same method that was used for preparing recombinant S1s (*19*).

Stopped-Flow Experiments. Stopped-flow experiments were performed using an SF61-DX2 stopped-flow spectrophotometer (Hi-Tech Scientific, Salisbury, U.K.) with a 75 W Xe/Hg lamp, as described previously (*12*).

Fluorescence Measurements. Steady-state fluorescence was measured using an F-4500 fluorescence spectrophotometer (Hitachi, Tokyo, Japan). CFP (donor) was excited at 433 nm, and its emitted spectra were recorded from 450 to 600 nm. Efficiencies (E) were calculated from donor fluorescence quenching at 475 nm as $1 - F_{DA}/F_D$, where F_{DA} is the fluorescence of the C/Y-S1 and F_D is the fluorescence of S1 fused by CFP only. CFP and YFP were treated as point masses. The distance between CFP and YFP fluorophores was calculated using the Förster equation (*21*, *22*), where $R = R_0(1/E - 1)^{1/6}$. The Förster distance, R_0, was calculated as $R_0 = (8.8 \times 10^{-23})(Q_D\kappa^2 n^{-4} J)^{1/6}$, where J is the overlap integral between CFP and YFP attached to the S1 expressed in M^{-1} cm^3 ($J = 2.18 \times 10^{-13}$), κ^2 is the orientation factor (assumed to be 0.667), n is the refractive index (assumed to be 1.4), and Q_D is the quantum yield (0.4 for CFP) obtained from the manufacturer's manual (Clontech). The calculated R_0 was 4.86 nm.

In Vitro Motility Assay. A motility assay was performed as described previously (*17*). Briefly, after the RLC was phosphorylated by myosin light chain kinase, myc-tagged HMMs were allowed to bind to the nitrocellulose-coated glass surface of the flow cell by using a monoclonal antibody against c-myc (9E10, Pharmingen, San Diego, CA); 8 μL of the concentrated antibody solution (0.3 mg/mL) was used to create a dense HMM surface, and 8 μL of the diluted solution (0.075 mg/mL) was used to create a sparse HMM surface. Actin filaments labeled with rhodamine phalloidin were infused into the flow cell, and the sliding movement of actin filaments in the presence of ATP was observed using an epifluorescence inverted IX70 microscope (Olympus, Tokyo, Japan) equipped with a rhodamine filter set.

Optical Tweezers and Nanometry. We used an inverted fluorescence IX71 microscope (Olympus) equipped with optical tweezers (Sigma Koki, Tokyo, Japan) and a quadrant photodetector (Sentech, Osaka, Japan) (*23*, *24*). Optical tweezers were used to independently control two polystyrene beads. Experiments were performed in a flow cell made from two parallel coverslips. Polystyrene beads (2 μm) were decorated sparsely with myc-tagged phosphorylated HMMs using anti-c-myc antibody. The beads were allowed to bind to the nitrocellulose-coated coverslip surface in a solution containing 25 mM KCl, 5 mM $MgCl_2$, and 20 mM HEPES (pH 7.8). The solution was replaced with one containing rhodamine phalloidin-labeled actin filaments and 1 μm polystyrene beads that had been precoated with α-actinin. A single actin filament was attached at either end to a bead held in the optical tweezers. Interactions between actin and the surface-bound HMM were monitored by projecting the image of one of the beads onto the center of a quadrant photodetector after enlarging it 10^3 times. In the assay, the solution was supplemented with 1−10 μM ATP, 0.5% (v/v) 2-mercaptoethanol, and an oxygen-scavenger system (glucose oxidase, catalase, and glucose). The stiffness of the laser trap was calculated from the variance of the Brownian motion of the trapped bead, using the equipartition law, $^1/_2K\langle X^2\rangle = {}^1/_2K_bT$, where K is stiffness, $\langle X^2\rangle$ is the standard deviation of the bead position, K_b is Boltzmann's constant, and T is temperature.

RESULTS

Mutations Do Not Significantly Affect the Early or Late States of ATP Hydrolysis. The question of whether a perturbation affects the very early stages of the myosin process is best answered by comparing the performance of a mutated system with the wild-type system, focusing on the early rate constants that characterize each system. The

Table 1: Rate Constants and Extents of Interaction with Nucleotides and Actin in Wild-Type and Mutant HMMs

	parameter	wild type	F721A	F775A
mant-ATP binding[a]	increase (%)	100	104	104
	K_1k_2 (s^{-1} M^{-1})	3.3×10^5	3.3×10^5	3.2×10^5
Trp fluorescence[a]	increase (%)	18	14	13
	K_1k_2 (s^{-1} M^{-1})	2.7×10^5	1.9×10^5	2.1×10^5
	k_{max} (s^{-1})	230	large	130
	$K_{0.5}$ (mM)	1	large	0.7
mant-ADP release[a]	k_5 (s^{-1})	1.3	1.5	1
basic ATPase[b]	k_{cat} (s^{-1})	0.023 ± 0.001	0.058 ± 0.010	0.043 ± 0.001
actin-activated ATPase[c]	V_{max} (s^{-1})	2.1 ± 0.3	0.71 ± 0.02	2.0 ± 0.1
	K_{actin} (mM)	0.050 ± 0.012	0.043 ± 0.004	0.053 ± 0.007

[a] Conditions: 0.45 M KCl, 2 mM $MgCl_2$, and 20 mM Tris-HCl (pH 7.5) at 20 °C. [b] Conditions: 0.45 M KCl, 2 mM $MgCl_2$, and 20 mM Tris-HCl (pH 7.5) at 25 °C. [c] Conditions: 0.01 M KCl, 2 mM $MgCl_2$, and 20 mM Tris-HCl (pH 7.5) at 25 °C.

constants are given as k_i, k_{-i}, and K_i ($i = 1, 2, ...$) in the B−T chemical kinetic scheme (*10*, *11*) (Scheme 1[2]).

Scheme 1

$$M + ATP \underset{k_{-1}}{\overset{k_1}{\rightleftarrows}} M{\cdot}ATP \underset{k_{-2}}{\overset{k_2}{\rightleftarrows}} M^*{\cdot}ATP \underset{k_{-3}}{\overset{k_3}{\rightleftarrows}} M^{**}{\cdot}ADP{\cdot}P_i \underset{k_{-4}}{\overset{k_4}{\rightleftarrows}} M^*{\cdot}ADP \underset{k_{-5}}{\overset{k_5}{\rightleftarrows}} M + ADP$$

The constants for the first process were experimentally measured using 2′(3′)-*O*-(*N*-methylanthraniloyl)adenosine 5′-triphosphate (mant-ATP) (*25*) in place of ATP so that the occupation of the active site can be inferred from the fluorescence emitted by the bound mant-ATP. Using mutant systems, addition of excess mant-ATP produced essentially the same increases in fluorescence that the wild-type system did (Table 1). The second-order rate constants (K_1k_2), estimated from the slope of the plots of the observed rate constant (k_{obs}) versus mant-ATP concentration, were very similar in the wild-type and mutant systems (Table 1). The second process, which was the conversion of M·ATP to M*·ATP, was measured directly in the three systems using the fact that Trp-512, located at the distal tip of the relay helix within the motor domain (*6*), enhances its fluorescence when the influence traveling from the active site reaches the helix (*15*, *26*, *27*). Upon addition of excess ATP, the increase in the Trp fluorescence for the mutant systems was only slightly smaller than that in the wild-type system (Table 1). Time transients of the fluorescence increase could be well fitted by a single exponential. The k_{obs} values were linearly dependent on ATP concentration at low ATP concentrations. The K_1k_2 values for the mutant systems were similar to those estimated from the development of mant fluorescence and close to the K_1k_2 value obtained for the wild-type system (Table 1).

However, the k_{obs} values were no longer linearly dependent on ATP concentration at greater ATP concentrations, in which range the dependence became quasi-hyperbolic [$k_{obs} \simeq k_{max}[ATP]/([ATP] + K_{0.5})$]. In the wild-type system, it is known that k_{max} corresponds to the rate of the hydrolytic transition (process 3 in the B−T sequence) (*28*). In the F775A system, the values of both k_{max} and $K_{0.5}$ were similar to those of the wild-type system; however, these parameters were too large to be measured in the F721A system (Table 1). It will be shown later that the mechanical linkage between the SH1 helix and the converter is completely disrupted in the F721A system. Normally, the acceleration of movement of the relay helix is slowed by the mass of the lever arm linked to the relay helix via the converter. We therefore may speculate that the large value of $k_3 + k_{-3}$ for the F721A system is the result of the faster movement of its relay helix, which is unregulated by the mass of the converter−lever arm system. We conclude that neither of our two perturbations significantly affects the events leading up to the arrival of the influence at the converter.

We also investigated whether the perturbations affected the two slow transitions (processes 4 and 5 in the B−T sequence) by measuring in each of the three systems the steady-state ATPase activity, and the rate of displacement of mant-ADP from the HMM·mant-ADP complex with excess ATP. The ATPase activities (k_{cat}) and the displacement rates (k_5) were similar in all three systems (Table 1). Moreover, it is interesting to note that the mutated systems exhibit actin activation (V_{max}) similar to that of the wild-type system (although F721A shows slightly lower levels), and that the K_{actin} values are also similar (Table 1). Together, the foregoing results show that the perturbations to be described next are specific effects produced on the converter, and not on any other element in the sequence.

Mutations Affect Movements of the Converter and the Lever Arm. For the first performance test of whether the mutations affect the lever arm movement, we constructed a test device, a chimeric S1[3] (C/Y-S1) in which YFP is fused to the N-terminus of the S1 heavy chain and CFP is fused to the N-terminus of the ELC. Because the CFP-to-YFP energy transfer between these fluorophores is well-understood and depends selectively on the distance between them, it is possible to detect their separation using optical measurements alone (*21*, *29*). Excitation of CFP at 433 nm resulted in a cyan emission at 450−515 nm, and the fluorescence energy transfer resulted in a yellow emission at 515−600 nm. When ATP or ADP was added to the wild-type C/Y-S1, the cyan emission from CFP decreased while the yellow emission from YFP increased (Figure 1A). The distance between the fluorophores decreased from 7.4 to 6.2 nm upon addition of ATP, and to 6.9 nm upon addition of ADP (Table 2). The distance between the termini, which was estimated

[2] In chemical notation, M stands for the truncated double-headed myosin that was used in our experiments, which is usually called HMM. Conformers of this protein, which can be distinguished by their absorbance or fluorescence, are denoted with one or two asterisks. As usual, k_i and k_{-i} are the forward and reverse rate constants, respectively of the ith reaction.

[3] To simplify the system, the single head of myosin, which is called S1, was used in this experiment.

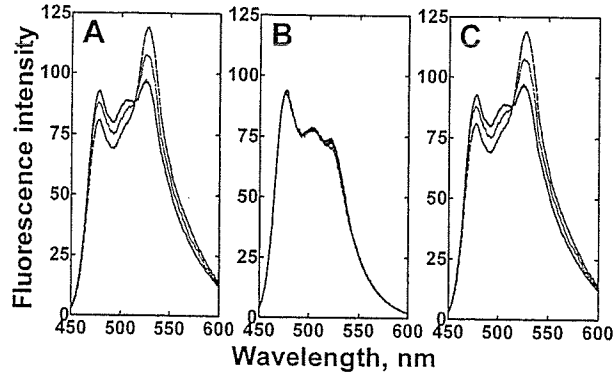

FIGURE 1: Fluorescence resonance energy transfer emission spectra. Emission spectra of wild-type (A), F721A (B), and F775A (C) C/Y-S1s excited at 433 nm were obtained in the absence of nucleotide (—), in the presence of 1 mM ATP (– – –), or in the presence of 0.1 mM ADP (···). Conditions:. 0.1 μM C/Y-S1s, 0.45 M KCl, 2 mM $MgCl_2$, 50 mM Tris-HCl (pH 8.0), and 0.5 mM dithiothreitol at 25 °C.

Table 2: Distances between CFP and YFP in Wild-Type and Mutant C/Y-S1s

C/Y-S1	nucleotide	FRET efficiency	distance (nm)
wild type	none	0.079 ± 0.010	7.4 ± 0.2
	ATP	0.183 ± 0.012	6.2 ± 0.1
	ADP	0.107 ± 0.008	6.9 ± 0.1
F721A	none	0.070 ± 0.005	7.3 ± 0.1
	ATP	0.082 ± 0.007	7.4 ± 0.1
	ADP	0.079 ± 0.001	7.4 ± 0.1
F775A	none	0.087 ± 0.002	7.5 ± 0.1
	ATP	0.201 ± 0.014	6.1 ± 0.1
	ADP	0.114 ± 0.024	6.9 ± 0.4

from the crystal structure of the motor domain complexed with an ATP analogue, was ~1.0 nm shorter than that estimated on the unligated motor domain (*3*, *7*). Therefore, the movement observed using the CFP fluorophore correlates well with the movement of the lever arm. When either ATP or ADP was added to the F721A C/Y-S1, there was no change in the energy transfer between the fluorophores (Figure 1B and Table 2). However, when these additions were made to the F775A C/Y-S1, the energy transfer changed just as it did in the wild-type C/Y-S1 (Figure 1C and Table 2). These results indicate that when either the wild-type or the F775A system undergoes the transition from the M to the M** state (see Scheme 1), it swings its lever arm, whereas the F721A system does not.

While the previous test examined the movement that myosin uses in carrying out its functions, the next two sample what is presumably the teleological function of myosin. We tested the speed at which actin is propelled [using a motility assay (*30*, *31*)], modulating the test severity by varying the resistance offered to its movement. On a surface that was densely covered with HMM molecules, the wild-type system propelled actin filaments at a speed of 0.51 ± 0.05 μm/s, but neither of the mutant systems moved actin filaments at all (Figure 2A). On a sparsely covered surface, the F721A system remained unable to propel actin filaments (Figure 2B). Surprisingly, however, we detected a slow movement of filaments by the F775A system (average velocity of 0.07 μm/s) under these conditions (Figure 2B). This indicates that although the F775A mutant retains the ability to swing its lever arm, its motor function is very weak. Mixing equal amounts of either F721A or F775A and the wild-type system

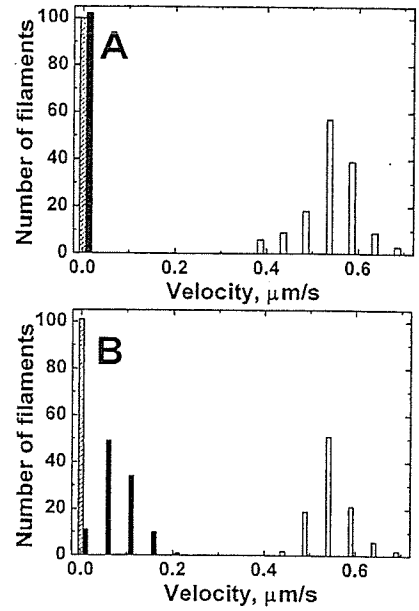

FIGURE 2: Distributions of the velocity of movement of actin filaments on glass surfaces densely (A) and sparsely (B) coated with HMMs: wild-type (empty), F721A (hatched), and F775A (filled). Conditions: 25 mM KCl, 3 mM $MgCl_2$, 20 mM HEPES (pH 7.8), and 2 mM ATP at 30 °C.

did not decrease the contribution of the wild-type component, indicating that the reduced motility expresses an inability of the mutant to generate force, but not irreversible binding of mutant dead heads to the actin filaments (data not shown).

In a final test of the wild-type and two mutated systems, we studied directly the ability of individual HMM molecules to exert force on actin. A single actin filament that was held taut by optical tweezers was brought close to a static bead that was sparsely coated with HMM molecules, and its position in space was sensitively monitored by projecting the bright-field image of the bead attached to the end of the actin filament onto a quadrant photodiode (*23*, *24*). Using weak trapping forces, there was significant thermal motion, which was expressed as positional variance of the held bead, except when actin–HMM interactions occurred. The equilibrium position without interactions between actin and HMM was defined as zero displacement. Both the wild-type and mutant systems showed periods of such low variance (therefore high stiffness) in their records (Figure 3A–F). The distribution of bead positions during these periods was fitted to a Gaussian curve, and the shift of the curve peak from the zero displacement position was called the size of the power stroke (Figure 3G–L). Under moderate trapping forces (stiffness of 0.03 pN/nm per bead), the shifts for both mutant systems were nearly zero (Figure 3I,K), which was much less than that of the wild-type system (6.5 ± 0.6 nm, Figure 3G). This indicates that neither of the mutants exerted sufficient force to pull the bead after the interaction between actin and HMM occurred. Next, we attempted to detect the weaker forces by lowering the stiffness of each trap to 0.008 pN/nm per bead. Under these conditions, the F775A system was able to pull the bead, although its power stroke was somewhat smaller than that of the wild-type system (5.5 and 6.9 nm, respectively; panels L and H of Figure 3). However, the F721A system was still unable to displace the bead under these conditions, even when so weakly trapped (Figure 3J). Thus, the results of this direct measurement of force correlate

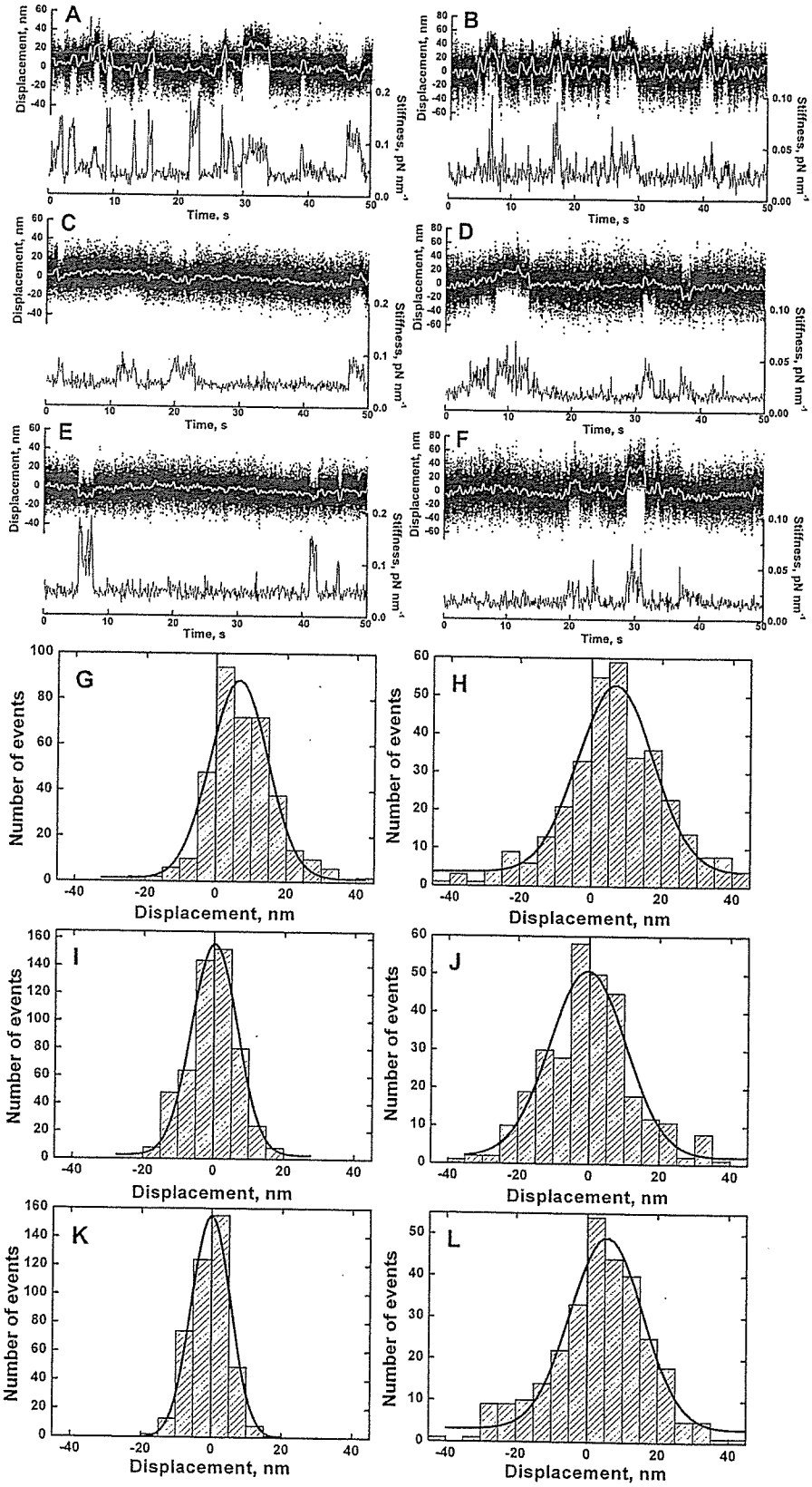

FIGURE 3: Displacements of actin filaments under moderately and extremely weak trapping forces caused by interactions with a single molecule of HMM. (A−F) In the data traces, the top traces show typical records of the displacements made by an HMM molecule at 1 μM ATP, the dots are raw data, the white lines are data passed through a low pass filter with a bandwidth of 2 Hz, and the bottom traces show stiffness calculated at intervals of 50 ms from the variance of the trapped bead position. (G−L) In the histograms of the displacements, solid vertical lines show the equilibrium (zero) position of the bead without interactions between actin and HMM. The fits to single Gaussian distributions are shown as solid lines. Mean sizes of the power stroke are 6.5 ± 0.6 nm for panel G, 6.9 ± 0.7 nm for panel H, 0.2 ± 0.4 nm for panel I, −0.4 ± 0.5 nm for panel J, −0.1 ± 0.4 nm for panel K, and 5.5 ± 0.7 nm for panel L. The trapping stiffness of each bead was 0.03 pN/nm for a moderately weak trapping force (A, C, E, G, I, and K) and 0.008 pN/nm for an extremely weak trapping force (B, D, F, H, J, and L). HMMs: wild-type (A, B, G, and H), F721A (C, D, I, and J), and F775A (E, F, K, and L). Conditions: 25 mM KCl, 5 mM $MgCl_2$, 20 mM HEPES (pH 7.8), and 1−10 μM ATP at ~20 °C.

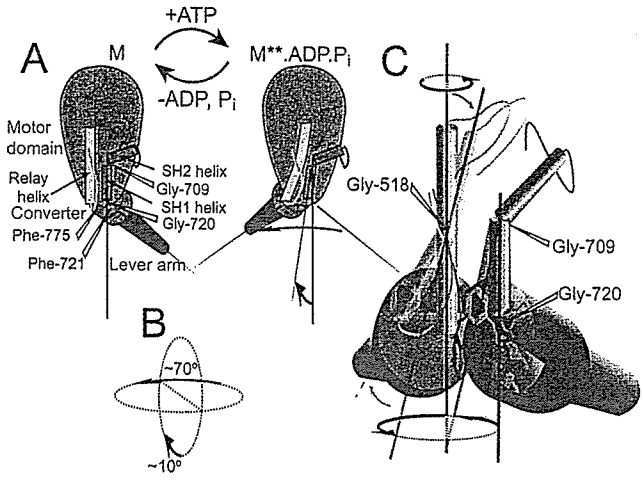

FIGURE 4: Mechanism by which motions within the motor domain are converted into a large rotation of the converter. (A) Lever arm swing. Myosin, initially in the M state (left), binds and rapidly hydrolyzes ATP to assume the metastable M**·ADP·P_i state (right). The relay helix and the SH1 (lower)/SH2 (upper) helices are shown as yellow and green rectangles, respectively. The ends of the relay helix are connected to the switch II loop (orange) and the converter (blue). The locations of Gly-709 (the flexible joint between the SH1 and SH2 helices), Gly-720 (the putative center for the rotation of the converter), and the two mutated residues (Phe-721 and Phe-775) are also shown. (B) ATP-induced conformational change, consisting of two almost perpendicular rotations. (C) Superimposition of nucleotide-free (the opaque image) and nucleotide-ligated (the translucent image) states. The converter and the lever arm are colored blue and purple, respectively. The switch II loop is shown as an orange strand, the relay loop as a silver strand, and the relay helix as a silver rod, and the SH1 (lower) and SH2 (upper) helices are shown as green rods. Arrows indicate the directions of shifts and rotations of the relay and SH1 helices that are induced by the closure of the nucleotide-binding cleft. The side chains of Phe-721 and Phe-775 are shown as red and pink hexagons, respectively. The β-sheet structure in the converter is shown as light-blue plane ribbons. The crystal structures of the skeletal muscle myosin with no nucleotide [Protein Data Bank (PDB) entry 2MYS] (*3*) and smooth muscle myosin complexed with MgADP·AlF_4^- (PDB entry 1BR4) (*7*) were adapted for the nucleotide-free and nucleotide-ligated myosin heads, respectively.

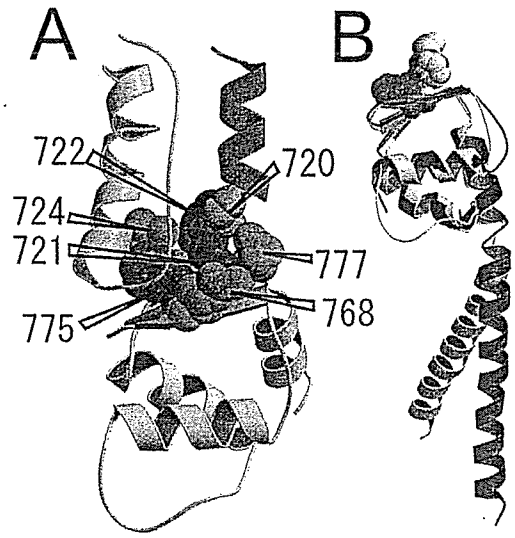

FIGURE 5: Structure and function of the small machine in the converter. (A) Enlarged view of the machine. The relay helix and loop are shown as a helical ribbon and a strand, respectively (both yellow). The SH1 helix is shown as a helical green ribbon. The three-stranded β-sheet is shown as plane ribbons (cyan), and all other structures in the converter are shown in white. Gly-720, Phe-721, Pro-722, Arg-724, Arg-768, Phe-775, and Arg-777 are presented as a CPK rendition. (B) Superposition of the converters in nucleotide-free and nucleotide-ligated myosin heads. In the former, the backbone atoms of the converter and a part of the lever arm are shown as blue and purple ribbons, respectively, and Gly-720 (orange), Phe-721 (red), and Phe-775 (pink) are presented as a CPK rendition. The latter is presented in the same manner, but all in white.

perfectly with those of the other performance tests (ability to swing the lever arm and to propel actin filaments in an *in vitro* motility assay), confirming that both mutations have special effects on the converter; the F775A mutation sharply inhibits its function but, unlike the F721A mutation, does not abolish it.

DISCUSSION

Since we can now refer to the three performance tests in Mutations Affect Movements of the Converter and the Lever Arm that report on the converter, we conclude that the two mutations had quite different effects on this element: the mutation at position 775 sharply inhibited its function, whereas the mutation at position 721 completely abolished it. We now describe the converter setting and its structure, and explain why these particular mutations were chosen. Thinking of the motor domain as fixed, we discuss the relative motion of the converter and the rigidly attached lever arm, focusing on the landmark of the SH1 helix (Figure 4A). The suggested movement of the converter when ATP is added to the distant active site is the sum of two almost perpendicular rotations: ~70° in the horizontal plane and ~10° in the vertical plane (*7*) (Figure 4B). These movements are enabled by the presence of Gly-720 (in the conserved Gly-Phe-Pro motif) at the helix−converter interface, and by Gly-709 of the helix (*7*). According to Rayment's studies of where crystal structures of the myosin head complexed with various ATP analogues belong in the catalytic cycle of ATP hydrolysis, the rotation of the converter domain occurs during the transition from the prehydrolysis state to the metastable state (ADP·P_i) after hydrolysis, or it occurs during the open-to-closed conformational change of the binding cleft (*5*, *6*, *32*, *33*).

The structure of the transmission system within the converter domain can be described in more detail as follows (Figure 5A). Three converter strands (residues 723−725, 766−770, and 773−777) form a β-sheet structure, and Phe-721 is in a compact hydrophobic cluster with Arg-768, Phe-775, and Arg-777 on the β-sheet. In the F721A system, the alanine substitute has no hydrophobic interaction with the cluster. The SH1 helix and the anterior part of the motor domain therefore lose contact with the converter stump and lever arm, which accounts for the uniform failure of this system in all of our tests of the lever arm swing and actin filament movements. In the F775A system, the normal hydrophobic interaction is absent, but Arg-724 and Arg-768 continue to form salt bridges with the relay helix; this might explain how the mutant continues to swing the lever arm and, albeit weakly, to move actin filaments. In normal operation, the side chain of Phe-775 is perpendicular to that of Phe-721, and makes direct contact with the distal end of the relay helix and the adjacent loop containing the ATP-sensitive Trp-512. These considerations suggest that, during the power stroke, the relay helix pushes the side chain of

Phe-775 with its tip, and rotates it around the principal axis of the SH1 helix.

We have further explored this speculation by comparing the structure of the relevant region (Gly-Phe-Pro motif and Phe-775) in its nucleotide-free and nucleotide-ligated states. The comparison reveals a largely unchanged structure, with the exception of a limited region in which a very small machine that accomplishes transmission seems to operate. The superimposition of images, as seen from the converter, reveals a rotation of ~70° around the principal axis of the SH1 helix in this area (Figure 4C and Movie S1 of the Supporting Information). Some movements are also observed near the relay helix and the SH1 helix. The rotation of this small machine is produced by the coordinated twisting motions of the two helices (circled arrows at the bottom), and further by the bending of the relay helix (translucent arrow). These motions of the transmission system can be created by the large Ramachandran angle changes at Gly-518 of the relay loop and at Gly-709 of the SH1 helix (*7*). The comparison between two converter structures in the nucleotide-free and nucleotide-ligated states revealed a high degree of similarity between states (Figure 5B), suggesting that the motion of the whole converter domain can largely be expressed as that of the little machine consisting of the Gly-Phe-Pro motif and Phe-775. Therefore, we suggest that this little machine is particularly important in positioning the converter–lever arm system. Other parts of the motor domain (for instance, the seven-stranded β-sheet structure core and the 25 kDa N-terminal domain) are also involved in the transmission of the force from the active site to the converter, but they seem to function as independent components of the overall motion.

Improved understanding of how the converter works gives a perspective of how overall transmission across myosin occurs. Closure of the cleft, which is induced by binding of the nucleotide to the active site, shifts the proximal end of the relay helix toward the active site (opaque arrow in Figure 4C), causing a clockwise rotation (as seen from the converter) (*5*, *34*). These movements cause a large rotation of the little machine consisting of two Phe residues linked to a Gly, through the cooperation of the relay helix, the relay loop, and the SH1 helix. Finally, this rotation is transmitted to the rigidly attached lever arm by the converter. *In situ*, the relay helix transmits mechanical changes in both the actin-detached and actin-attached states (during the reverse and power strokes, respectively) (*13*, *21*). However, under the circumstances that we describe, force is generated more effectively during the power stroke than during the reverse stroke. This is because the former occurs through a pushing motion of the side chain of Phe-775, whereas the latter occurs through a pulling motion, perhaps using hydrophobic interactions between the relay helix and the converter.

ACKNOWLEDGMENT

We thank K. Konishi for her early contribution to this study and T. Yanagida, H. Tanaka, and T. Watanabe for helping us assemble a microscope equipped with laser tweezers and a quadrant photodetector. We also thank T. J. Pearson for significant improvements to our manuscript.

SUPPORTING INFORMATION AVAILABLE

Movie showing a schematic three-dimensional model of the actions of the transmission machinery of myosin. This material is available free of charge via the Internet at http://pubs.acs.org.

REFERENCES

1. Huxley, H. E. (1969) The mechanism of muscular contraction, *Science 164*, 1356–1365.
2. Huxley, A. F., and Simmons, R. M. (1971) Proposed mechanism of force generation in striated muscle, *Nature 233*, 533–538.
3. Rayment, I., Rypniewski, W. R., Schmidt-Bäse, K., Smith, R., Tomchick, D. R., Benning, M. M., Winkelmann, D. A., Wesenberg, G., and Holden, H. M. (1993) Three-dimensional structure of myosin subfragment-1: a molecular motor, *Science 261*, 50–58.
4. Rayment, I., Holden, H. M., Whittaker, M., Yohn, C. B., Lorenz, M., Holmes, K. C., and Milligan, R. A. (1993) Structure of the actin-myosin complex and its implications for muscle contraction, *Science 261*, 58–65.
5. Fisher, A. J., Smith, C. A., Thoden, J. B., Smith, R., Sutoh, K., Holden, H. M., and Rayment, I. (1995) X-ray structures of the myosin motor domain of *Dictyostelium discoideum* complexed with MgADP·BeF_x and MgADP·AlF_4^-, *Biochemistry 34*, 8960–8972.
6. Smith, C. A., and Rayment, I. (1996) X-ray structure of the magnesium(II)·ADP·vanadate complex of the *Dictyostelium discoideum* myosin motor domain to 1.9 Å resolution, *Biochemistry 35*, 5404–5417.
7. Dominguez, R., Freyzon, Y., Trybus, K. M., and Cohen, C. (1998) Crystal structure of a vertebrate smooth muscle myosin motor domain and its complex with the essential light chain: visualization of the pre-power stroke state, *Cell 94*, 559–571.
8. Houdusse, A., Szent-Györgyi, A. G., and Cohen, C. (2000) Three conformational states of scallop myosin S1, *Proc. Natl. Acad. Sci. U.S.A. 97*, 11238–11243.
9. Holmes, K. C., Angert, I., Kull, F. J., Jahn, W., and Schröder, R. R. (2003) Electron cryo-microscopy shows how strong binding of myosin to actin releases nucleotide, *Nature 425*, 423–427.
10. Bagshaw, C. R., and Trentham, D. R. (1974) The characterization of myosin-product complexes and of product-release steps during the magnesium ion-dependent adenosine triphosphatase reaction, *Biochem. J. 141*, 331–349.
11. Bagshaw, C. R., Eccleston, J. F., Eckstein, F., Goody, R. S., Gutfreund, H., and Trentham, D. R. (1974) The magnesium ion-dependent adenosine triphosphatase of myosin. Two-step processes of adenosine triphosphate association and adenosine diphosphate dissociation, *Biochem. J. 141*, 351–364.
12. Onishi, H., Ohki, T., Mochizuki, N., and Morales, M. F. (2002) Early stages of energy transduction by myosin: roles of Arg in switch I, of Glu in switch II, and of the salt-bridge between them, *Proc. Natl. Acad. Sci. U.S.A. 99*, 15339–15344.
13. Onishi, H., Mochizuki, N., and Morales, M. F. (2004) On the myosin catalysis of ATP hydrolysis, *Biochemistry 43*, 3757–3763.
14. Malnasi-Csizmadia, A., Woolley, R. J., and Bagshaw, C. R. (2000) Resolution of conformational states of *Dictyostelium* myosin II motor domain using tryptophan (W501) mutants: implications for the open-closed transition identified by crystallography, *Biochemistry 39*, 16135–16146.
15. Malnasi-Csizmadia, A., Kovacs, M., Woolley, R. J., Botchway, S. W., and Bagshaw, C. R. (2001) The dynamics of the relay loop tryptophan residue in the *Dictyostelium* myosin motor domain and the origin of spectroscopic signals, *J. Biol. Chem. 276*, 19483–19490.
16. Yanagisawa, M., Hamada, Y., Katsuragawa, Y., Imamura, M., Mikawa, T., and Masaki, T. (1987) Complete primary structure of vertebrate smooth muscle myosin heavy chain deduced from its complementary DNA sequence. Implications on topography and function of myosin, *J. Mol. Biol. 198*, 143–157.
17. Kojima, S., Fujiwara, K., and Onishi, H. (1999) SH1 (cysteine 717) of smooth muscle myosin: its role in motor function, *Biochemistry 38*, 11670–11676.
18. Kunkel, T. A., Roberts, J. D., and Zakour, R. A. (1987) Rapid and efficient site-specific mutagenesis without phenotypic selection, *Methods Enzymol. 154*, 367–382.

19. Konishi, K., Kojima, S., Katoh, T., Yazawa, M., Kato, K., Fujiwara, K., and Onishi, H. (2001) Two new modes of smooth muscle myosin regulation by the interaction between the two regulatory light chains, and by the S2 domain, *J. Biochem. 129*, 365−372.
20. Onishi, H., Maéda, K., Maéda, Y., Inoue, A., and Fujiwara, K. (1995) Functional chicken gizzard heavy meromyosin expression in and purification from baculovirus-infected insect cells, *Proc. Natl. Acad. Sci. U.S.A. 92*, 704−708.
21. Suzuki, Y., Yasunaga, T., Ohkura, R., Wakabayashi, T., and Sutoh, K. (1998) Swing of the lever arm of a myosin motor at the isomerization and phosphate-release steps, *Nature 396*, 380−383.
22. Stryer, L. (1978) Fluorescence energy transfer as a spectroscopic ruler, *Annu. Rev. Biochem. 47*, 819−846.
23. Finer, J. T., Simmons, R. M., and Spudich, J. A. (1994) Single myosin molecule mechanics: piconewton forces and nanometre steps, *Nature 368*, 113−119.
24. Molloy, J. E., Burns, J. E., Kendrick-Jones, J., Tregear, R. T., and White, D. C. (1995) Movement and force produced by a single myosin head, *Nature 378*, 209−212.
25. Hiratsuka, T. (1983) New ribose-modified fluorescent analogs of adenine and guanine nucleotides available as substrates for various enzymes, *Biochim. Biophys. Acta 742*, 496−508.
26. Batra, R., and Manstein, D. J. (1999) Functional characterization of *Dictyostelium* myosin II with conserved tryptophanyl residue 501 mutated to tyrosine, *Biol. Chem. 380*, 1017−1023.
27. Onishi, H., Konishi, K., Fujiwara, K., Hayakawa, K., Tanokura, M., Martinez, H. M., and Morales, M. F. (2000) On the tryptophan residue of smooth muscle myosin that responds to binding of nucleotide, *Proc. Natl. Acad. Sci. U.S.A. 97*, 11203−11208.
28. Marston, S. B., and Taylor, E. W. (1980) Comparison of the myosin and actomyosin ATPase mechanisms of the four types of vertebrate muscles, *J. Mol. Biol. 139*, 573−600.
29. Majoul, I., Straub, M., Duden, R., Hell, S. W., and Soling, H. D. (2002) Fluorescence resonance energy transfer analysis of protein−protein interactions in single living cells by multifocal multiphoton microscopy, *J. Biotechnol. 82*, 267−277.
30. Harada, Y., Noguchi, A., Kishino, A., and Yanagida, T. (1987) Sliding movement of single actin filaments on one-headed myosin filaments, *Nature 326*, 805−808.
31. Kron, S. J., and Spudich, J. A. (1986) Fluorescent actin filaments move on myosin fixed to a glass surface, *Proc. Natl. Acad. Sci. U.S.A. 83*, 6272−6276.
32. Gulick, A. M., Bauer, C. B., Thoden, J. B., and Rayment, I. (1997) X-ray structures of the MgADP, MgATPγS, and MgAMPPNP complexes of the *Dictyostelium discoideum* myosin motor domain, *Biochemistry 36*, 11619−11628.
33. Bauer, C. B., Holden, H. M., Thoden, J. B., Smith, R., and Rayment, I. (2000) X-ray structures of the apo and MgATP-bound states of *Dictyostelium discoideum* myosin motor domain, *J. Biol. Chem. 275*, 38494−38499.
34. Fisher, A. J., Smith, C. A., Thoden, J., Smith, R., Sutoh, K., Holden, H. M., and Rayment, I. (1995) Structural studies of myosin:nucleotide complexes: a revised model for the molecular basis of muscle contraction, *Biophys. J. 68*, 19S−26S.

BI048954F

BIOCHEMISTRY

Volume 43, Number 13 April 6, 2004

Current Topics

On the Myosin Catalysis of ATP Hydrolysis†

Hirofumi Onishi,*,‡ Naoki Mochizuki,‡ and Manuel F. Morales§

Department of Structural Analysis, National Cardiovascular Center Research Institute, Fujishiro-dai, Suita, Osaka 565-8565, Japan, and University of the Pacific, San Francisco, California 94115 USA

Received January 6, 2004; Revised Manuscript Received February 3, 2004

ABSTRACT: Myosin is an ATP-hydrolyzing motor that is critical in muscle contraction. It is well established that in the hydrolysis that it catalyzes a water molecule attacks the γ-phosphate of an ATP bound to its active site, but the details of these events have remained obscure. This is mainly because crystallographic search has not located an obvious catalytic base near the vulnerable phosphate. Here we suggest a means whereby this dilemma is probably overcome. It has been shown [Fisher, A. J., et al. (1995) *Biochemistry 34*, 8960−8972; Smith, C. A., and Rayment, I. (1996) *Biochemistry 35*, 5404−5417] that in an early event, Arg-247 and Glu-470 come together into a "salt-bridge". We suggest that in doing so they also position and orient two contiguous water molecules; one of these becomes the lytic water, perfectly poised to attack the bound γ-phosphorus. Its hydroxyl moiety attacks the phosphorus, and the resulting proton transfers to the second water, converting it into a hydronium ion (as is experimentally observed). It is shown in this article how these central events of the catalysis are consistent with the behavior of several residues of the neighboring region.

Myosin is the key enzyme in transducing the free energy of ATP hydrolysis into the directed movements of adjoining actin filaments, so it is central in "muscle contraction". The aim of this article is to suggest what parts of myosin execute catalysis, and how such catalysis proceeds.[1] The "story" we develop arises in part from our mutational studies (*1*−*3*) but is heavily dependent on the crystallographic studies of Rayment et al. (*4*−*6*), and more recently those of Cohen et al. (*7*, *8*). The importance of explaining myosin catalysis has been evident. But as Rayment (*5*) has pointed out, progress has been thwarted because there appears to be no (necessary) proton acceptor within 5.5 Å of the vulnerable P−O linkage of bound ATP; nevertheless, we have paid attention to Rayment's note of a "water network" (*6*). Also, we have learned much from analogizing with the G-protein system that catalyzes the hydrolysis of GTP (*9*−*11*). Our program here is to present a reasonable hypothesis about events that

† This work was supported by Grant-in-Aids for Scientific Research and by Special Coordination Funds for Promoting Science and Technology from the Ministry of Education, Culture, Sports, Science, and Technology (to H.O. and N.M.) and by Grant MCB 9603670 from the National Science Foundation (to M.F.M.). A condensed version of this study was presented at the annual meeting of the American Biophysical Society held in San Antonio, Texas on March 2, 2003 (*Biophys. J.* 84, No. 2, Part 2 of 2, 3a, 2003).

* Address correspondence to this author: Tel: +81-6-6833-5012. Fax: +81-6-6872-8092. E-mail: honishi@ri.ncvc.go.jp.

‡ National Cardiovascular Center Research Institute.

§ University of the Pacific.

[1] In muscle contraction, a second protein, actin, is an essential partner, which, in addition to substrate, interacts with myosin. However, myosin alone is able to catalyze ATPase, and it is to this simplified system (myosin + substrate + ions + water) that this article refers. When actin is also present, the rates at which myosin conducts various processes that comprise its catalysis are very different. It is logically possible that the qualitative nature of its catalysis inside its catalytic cleft is then also different; however, because even in the presence of actin, hydrolysis occurs after myosin has released from actin, and myosin rebinds actin at its M**·ADP·P_i state, such a circumstance seems very unlikely, but should be kept in mind.

10.1021/bi040002m CCC: $27.50
Published on Web 03/06/2004

Scheme 1

$$M+ATP \overset{1}{\rightleftarrows} M\cdot ATP \overset{2}{\rightleftarrows} M^{*}\cdot ATP \overset{3}{\rightleftarrows} M^{**}\cdot ADP\cdot P_i$$

lead up to positioning the "lytic" water destined to attack the γ-phosphate moiety of myosin-bound ATP—along the way showing how nature probably supplies the "missing" proton acceptor.

Informational Background. We are especially concerned with the early events of myosin catalysis, beginning with what happens in the myosin molecule just after a nucleotide, such as ATP, binds to its "active site", and is being prepared for hydrolysis. In terms of the Trentham-Bagshaw kinetic scheme (*12*, *13*), these early events are described by Scheme 1 where M and P_i are myosin and inorganic phosphate, respectively, and * and ** indicate conformers distinguishable by absorbance (*14*) or fluorescence (*15*). Recent studies have identified the residue bearing the optical sensor as Trp-512[2] (*16*−*22*).

Rayment and his successors have begun to reconstruct the transformations of the hydrolyzing myosin-nucleotide system by successively taking crystallographic "snapshots" of the system in the order in which they think the real transformations occur (*5*, *6*, *23*). Of course, each snapshot has to be static, made by using, for example, a stable non-hydrolyzing intermediate thought to be analogous to the real intermediate. By such an approach, they have made intelligent guesses about the highly resolved structures in a succession of myosin states.

Building on the crystallography, we have, in parallel, tried to study the real system as it passes rapidly through the same transformations, attempting, by kinetic measurements, to sample *all* the states— among these the ones resolved in the snapshots. In applying our approach, however, we can use site-directed mutation, i.e., examine in the same way *various* systems, differing from each other in structure only at *one* residue position.[3] Comparison of the behavior of such systems, say the normal ("wild type") and a particular mutated system, often suggests something about the role of that residue in the normal system. What follows is a comprehensive hypothesis of how myosin catalysis works, based on our synthesis of crystallographic and conventional biochemical knowledge.

A graphic impression of how events of our interest begin is given by Figure 1, which also illustrates the "successive snapshot" logic used by crystallographers. It is thought that stable systems of ATP analogues, ADP·BeF_x and ADP·VO_4^-, respectively, are legitimate models from which to infer the behavior of molecules containing authentic ATP in the prehydrolytic and transition states, and in the presence of other participants in the system (*5*, *6*). With these provisos, we can portray what probably happens during a process in which the cleft region of myosin, having bound ATP, transits from one state to another. Understood is that the system as a whole suffers an accompanying free energy decrement. We cannot express such a change in structural detail, but a very notable item is that, in the process, two flexible loop residues— Arg-247 and Glu-470—initially remote from each other, come into a "salt-bridge". Seemingly as a result, the binding cleft closes over the bound substrate, and immediately, the distant Trp-512 responds by increasing its fluorescence. (Note that cleft and Trp-512 are connected by a long but rigid helix. It is for this reason that enhanced fluorescence is taken to signal cleft closing). Thereafter, the γ-phosphate of the bound nucleotide is in some way prepared for its catalyzed hydrolysis.

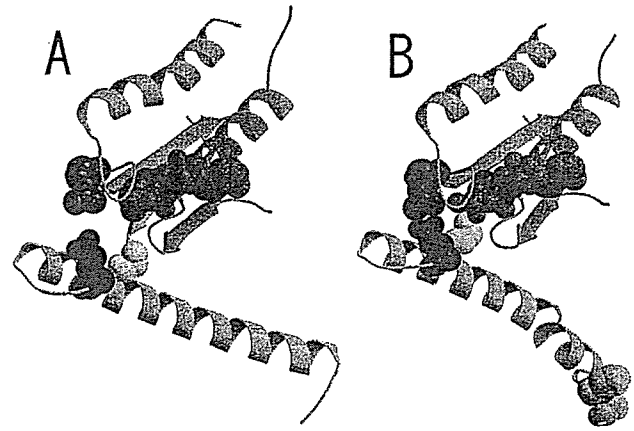

FIGURE 1: Ribbon representation of the nucleotide-binding pocket of the open (A) and closed (B) forms of myosin. Crystal structures of *Dictyostelium* myosin motor domain complexed with MgADP·BeF_x (ref *5*: PDB entry 1MMD) and MgADP·VO_4^- (ref *6*: PDB entry 1VOM) are adopted for the open and closed forms, respectively. Backbone atoms of the sequences of residues 167−203 (P-loop), 218−258 (Switch I), and 457−513 (Switch II) of the heavy chain are colored green, orange, and light blue, respectively. Bound nucleotides, Mg^{2+}, Arg-247, Gly-468, Glu-470, and Trp-512 are shown as space-filled balls in gray, dark green, red, yellow, blue, and violet, respectively. Note that a salt-bridge is formed between residues Arg-247 and Glu-470 in the closed form. Also note that in this form, Gly-468 is in contact with the γ-phosphate moiety of the bound nucleotide. The nucleotide-responsive tryptophan residue (Trp-512) is connected with the Switch II loop by a long α-helix.

Early on, Glu-470 interested us (*1*) because of its suspicious location near the γ-phosphate of the bound nucleotide, and even more later after Rayment (*5*, *6*) discovered the salt-bridge formation. To study the situation more deeply, we prepared and analyzed several mutant systems (*2*, *3*). In some, Arg-247 was replaced by Ala or Glu, and in some, Glu-470 was replaced by Ala or Arg. In one, the assignments of Arg and Glu were reversed to Glu and Arg. To track the systems in time (step 1 in Scheme 1), we used mantATP[4] instead of ATP, and for step 2, we used the equivalent fluorescence from Trp-512. In each case, we assessed the ability to hydrolyze nucleotide triphosphate by its production of inorganic phosphate (step 3). From these experiments, we drew many important conclusions (*2*, *3*), for example, that

[2] Although the amino acid sequence of a protein is different in various organisms (or in different major tissues of the same organism), well-established homologies permit interspecific translation from one species to another. Throughout, we use the sequence numeration appropriate for smooth muscle myosin, as extracted from chicken gizzard. We note that Lys-183, Thr-184, Asn-242, Asn-244, Ser-245, Ser-246, Arg-247, Asp-465, Ile-466, Ala-467, Gly-468, Glu-470, and Trp-512 correspond to *Dictyostelium discoideum* Lys-185, Thr-186, Asn-233, Asn-235, Ser-236, Ser-237, Arg-238, Asp-454, Ile-455, Ser-456, Gly-457, Glu-459, and Trp-501.

[3] The myosin properties of present concern all exist in the truncated, proteolytically obtainable, two-headed structure known as "heavy meromyosin", and used in our experiments, so we do not distinguish between our structure and truly intact myosin, for which "M" is intended to stand.

[4] Abbreviation: mantATP, 2′(3′)-*O*-(*N*-methylanthranilloyl) adenosine 5′-triphosphate.

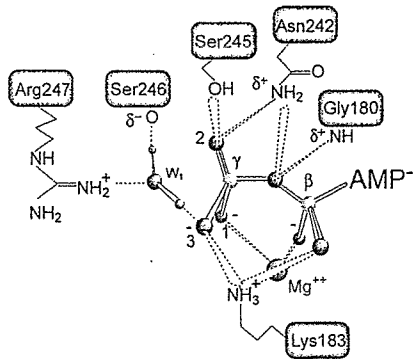

FIGURE 2: The structure of the prehydrolysis state (M·ATP). The γ-phosphate of ATP is in a tetrahedral arrangement with its four oxygen atoms. A water molecule involved in hydrogen bonding with the γ-phosphate is denoted as w_1. We assume that this water is HOH1181 in the Fisher et al. structure (ref *5*, 1MMD). The β- and γ-phosphate groups of ATP; Mg^{2+}, and the water molecule are shown in ball-and-stick form. Covalent bonds are shown as solid lines and hydrogen bonds and ionic interactions in dashed lines. Phosphorus, oxygen, hydrogen, and magnesium are depicted in yellow, red, blue, and green, respectively.

probably the electrical force between Arg-247 and the bound triphosphate moiety helps to close the cleft and to signal Trp-512. On the other hand, we felt that the close correlation between the presence of Glu at position 470 and hydrolysis probably meant that that particular residue had a role in catalysis. From the foregoing beginnings, we now commence to put together our hypothesis in the sequence that we suppose will be easiest to verify.

The Prehydrolytic State. Key features of relevant M·ATP structure, i.e., of the situation at the active site, are in Figure 2 (abstracted from a Rayment snapshot of bound MgADP·BeF_x). Three oxygen atoms (1, 2, and 3) of the γ-phosphate group are bound and oriented by bound Mg^{2+}, the side chains of Asn-242 ($N_{\delta 2}$) and Ser-245 (O_γ) of Switch I, and Lys-183 of the P-loop, respectively. A single molecule of water, w_1, is attached to the guanidino group of Arg-247 ($N_{\eta 1}$), which interacts with a main chain carbonyl oxygen of Ser-246 of Switch I, and is attached to oxygen (3) of the γ-phosphate moiety of the bound nucleotide. (Note: The orientation of w_1 is similar to that of a water molecule at the active site of transducin G_α complexed with GTPγS that mimics the ground state of bound GTP (*11*)). Because earlier we found a good correlation between the presence of Arg at position 247 and the rate of substrate binding to the active site (*3*), we speculated above that Arg-247 indirectly, perhaps by its electrical force, interacts with the γ-phosphate moiety via w_1, and so for this reason this positive residue is important for binding substrate to the active site. In this ground state, however, w_1 does not yet have the position to act (see below).

Closure of the Nucleotide-Binding Cleft. Figure 3 depicts diagrammatically how we think this cleft closes: (A) repeats the same stage depicted in Figure 2; (B) is an intermediate stage; and (C) is the final stage. Comparison of the three stages implies that on closure there is a big structural change in Switch II (in light blue), but none in Switch I (in black).

In Figure 3A the cleft is still open, so the Switch II residues, excepting Asp-465, do not interact with either the bound nucleotide or the bound Mg^{2+} at this stage. Mg^{2+} is very important in closure because of its location in the cleft. It is central in chelating the β- and γ-phosphates of the

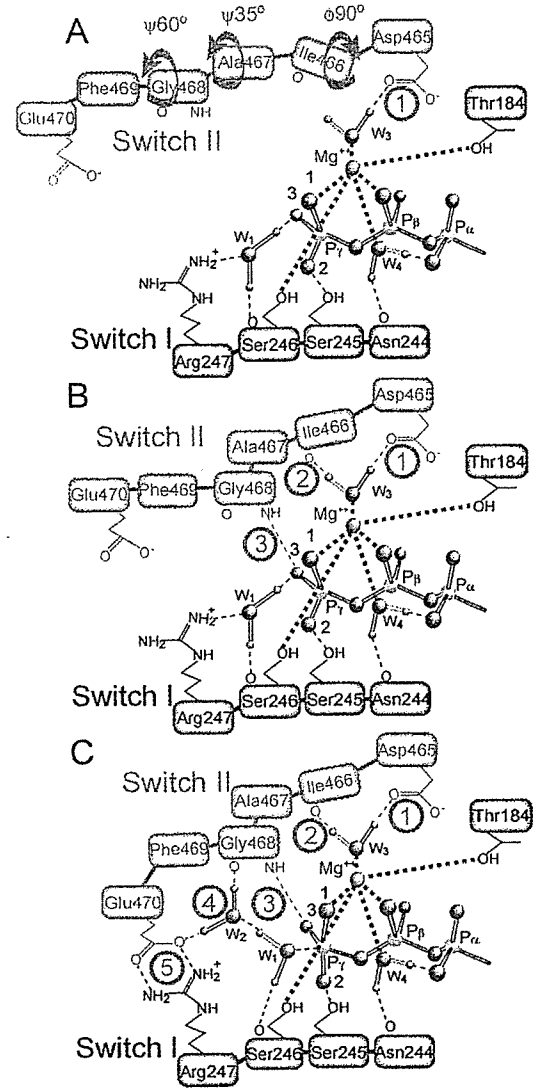

FIGURE 3: The closing process of the nucleotide-binding cleft. A series of diagrams show the disposition in space of the Switch II strand (colored light blue) at three different times after nucleotide binds to the active site: A, the early stage; B, the intermediate stage; and C, the final stage. In the diagrams, we also show how the γ-phosphate moieties of bound nucleotide are associated with the strand. We assume that w_1 in A is HOH1181 in the Fisher et al. structure (ref *5*, 1MMD) and that w_1 and w_2 in C take the place of the terminal oxygen atom of the vanadate moiety and that of HOH697, respectively, in the Smith and Rayment structure (ref *6*, 1VOM). Three curved arrows show the general direction in which relevant Ramachandran angles change in the transition from the A to the B state (the angle and the amount of its change are given). The progressive attachments of the Switch II strand occur in the sequence given by the circled numeral. Covalent bonds are shown as solid lines and hydrogen bonds and ionic interactions in dashed lines. Coordinated interactions with the Mg^{2+} of bound nucleotide are shown as green, thick dashed lines. Phosphorus, oxygen, hydrogen, and magnesium are depicted in yellow, red, blue, and green, respectively.

nucleotide, and in its coordination sphere are six ligands in octahedral geometry. Also, Mg^{2+} is connected with both the P-loop via $O_{\gamma 1}$ of Thr-184 and Switch I via O_γ of Ser-246. Two water molecules are coordinated to Mg^{2+}. One, w_4, interacts with the main chain carbonyl oxygen of Asn-244, and also bonds to an oxygen atom of the α-phosphate group. One of the hydrogen atoms of another water molecule, w_3, interacts with the side chain of Asp-465 ($O_{\delta 2}$). This fact,

and his own work on mutations, led Sutoh to suggest that Asp-465 is important in nucleotide binding (*24*). We propose that w_1 retains its attachment to Switch I, and that, by virtue of the intervention of w_3 (which inserts between the Mg^{2+} associated with Switch I via the bound nucleotide and a carboxyl oxygen atom of Asp-465 of Switch II), the closing of the cleft is initiated. The three curved arrows in Figure 3A indicate the direction in which the relative Ramachandran angles change in the transition between states. When Ile-466 rotates (permitted by the flexibility of the Switch II loop) in such a way that its Ramachandran angle ϕ increases by 90°, the oxygen atom of its main chain carbonyl group moves toward w_3, and can now form a bond with the other hydrogen atom of the w_3. Accompanying changes in the φ angles of Ala-467 and Gly-468 (see Figure 3A) create an interaction between the main chain amide hydrogen of Gly-468 and the γ-phosphate moiety of the bound nucleotide. (See Figure 3B.) At this stage, w_2 first appears in the crystallographic image of the phosphate pocket of the enzyme. It is hydrogen-bonded to the main chain carbonyl oxygen of Gly-468, and to one of the two oxygen atoms of the carboxyl group of Glu-470 ($O_{\epsilon 1}$). See Figure 3C. As earlier noted, Trp-512 is remotely connected to Switch II in the active site; it is at this stage that Trp-512 is "informed" and increases its fluorescence. (See Scheme 1.)

Although, strictly speaking, observations of the sort we are citing cannot be put in cause-to-effect relations, cleft closure is closely correlated in time with at least two other important events. One is that, with closure, force appears to be transmitted via the long α-helix, across the so-called "converter" region, to what appears to be the myosin "lever arm" (*7*). It is known that in a myosin "motor", the mechanical working (power) stroke is time-correlated with the phosphate release step that follows hydrolysis (Figure 4). Also, Sutoh et al. (*25*) showed that a large angle change of the lever arm occurring during M·ATP → M*·ATP is necessary for the reverse of the power stroke motion. Other events also associated with closure (to be discussed later) are a hydrogen-bond interaction between Gly-468 and an oxygen atom of the γ-phosphate, and the formation of the salt-bridge between side chains of Arg-247 and Glu-470—all crucial for setting up catalysis.

The Transition State for Hydrolysis. In the snapshot taken to represent the situation at the time of hydrolysis ($MgADP{\cdot}VO_4^-$ bound to the active site), the cleft is closed and there are two molecules of water bound in the γ-phosphate pocket (*6*). We suppose (Figure 3C) that movement of Glu-470 permits its bridging toward the guanidino group of Arg-247, which then releases its water, w_1, destined to become the "lytic" water. One of the hydrogen atoms of this water, initially bonded to an oxygen atom of the γ-phosphate group, then interacts with the oxygen atom of a new, intruding water, w_2. The other hydrogen atom remains bonded to the main chain carbonyl oxygen of Ser-246. A result of making this critical conjecture is that then w_1 ends up partially positioned and oriented to carry out its attack on the γ-phosphorus (cf., the analogous location of the lytic water in the active site of transition-state transducin G_α (*11*)). Even at this stage, however, our conjecture already responds to certain requirements. It provides explanations of why two water molecules are seen in the snapshot of the transition state (*6*), why the ability of a system to catalyze hydrolysis

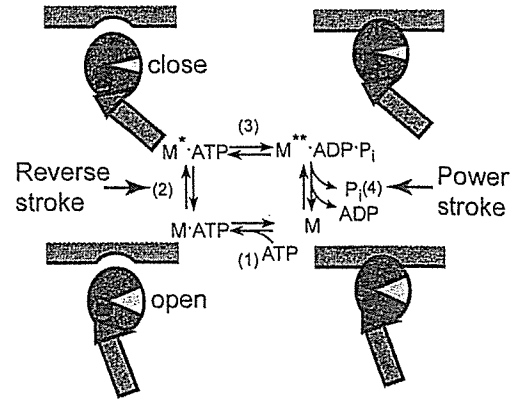

FIGURE 4: Some important transformations during the ATPase cycle. Chemically, myosin (M) binds to ATP, hydrolyzes it to ADP·P_i, and releases the products. To function in muscle contraction myosin must undergo (a) a conformational change that switches between actin-binding and actin-release states, and (b) a conformational change that swings the lever arm for contraction ("power stroke"). Presumably, a sequence that must occur in muscle is (1) the conformational change that allows release from actin, (2) the conformational change that reverse swings the lever arm, (3) the conformational change to the actin-binding state, and (4) the conformational change that swings the lever arm in the power stroke. In this article, however, we are only concerned with conformational change (2) and the following hydrolysis. As the product release from M**·ADP·P_i, at which the power stroke occurs, is greatly accelerated by actin, it seems reasonable to assume that the transition to the actin-binding state occurs in the state M**·ADP·P_i. However, the conformational change during this transition is not well clarified yet. The reverse and power strokes occur at the stages indicated. This figure also denotes the relationship of myosin to actin (free or bound). The motor domain is depicted in red, the converter in green, the lever arm in blue, the nucleotide-binding cleft in yellow, and the actin filament in violet. A long, conserved α-helix that connects between the binding cleft and the converter is shown as a spiral in the motor domain.

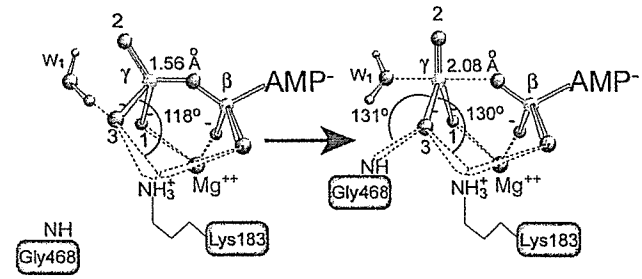

FIGURE 5: A mechanism for the change of the γ-phosphate configuration. The left and right diagrams represent the tetrahedral and the trigonal bipyramidal structures, respectively. The β- and γ-phosphate of ATP, the Mg^{2+}, and a water molecule are shown as a ball-and-stick model. Oxygen atoms interacted with Mg^{2+}, Ser-245, and Lys-183 are denoted as 1, 2, and 3, respectively. Angles of P_γ—O—N_ζ of Lys-183 and P_γ—O—$N_{main\ chain}$ of Gly-468, and the distance between the γ-phosphorus and the β—γ bridging oxygen are given from the crystal structures (1MMD for the left diagram and 1VOM for the right diagram).

is tightly correlated to the presence of Glu at position 470 (*3*), and why the Rayment (*6*) surmise of a functional role for a "water network" was prophetic.

Although already partly positioned by w_2 and Ser-246, we believe that w_1 is not yet at its final attack position and that its final positioning results from the shift of the γ-phosphate structure from its tetrahedral to its trigonal bipyramidal configuration. As already stated, we cannot assign cause-to-effect relationships, but do think that the final positioning

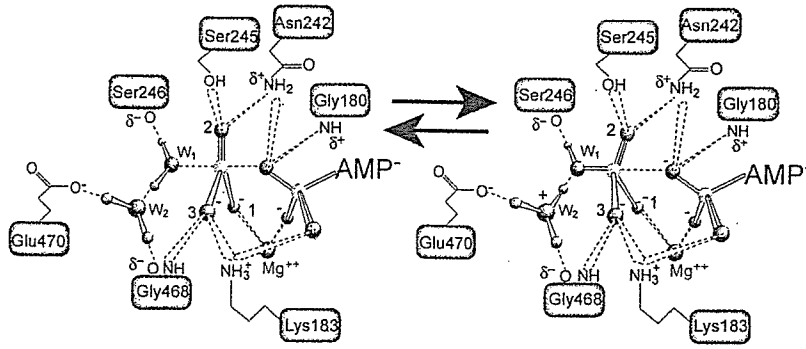

FIGURE 6: The transfer of a proton from w_1 to w_2 and the production of P_i and H_3O^+. The left and right diagrams represent the structures for the transition and posthydrolysis states, respectively. δ^+ and δ^- indicate positive and negative charges, respectively, which are induced by the resonance structures of the peptide bond. Covalent bonds are shown as filled lines, and hydrogen bonds and ionic interactions in dashed lines. The β- and γ-phosphates of ATP, Mg^{2+}, and two water molecules are shown as a ball-and-stick model.

ends a series of identifiable events. It will be recalled that Gly-468 is the only residue whose interaction with the γ-phosphate is induced by the cleft closure. One of possible speculations about the conformational change of the γ-phosphate now follows. As is well-known, the normal angle of separation between two oxygen bonds is about 105°. In the prehydrolysis state ($MgADP{\cdot}BeF_x$ bound to the active site), this angle in $P_\gamma-O-N_\zeta$ of Lys-183 is 118° (quasi normal) (left, Figure 5). So, we suggest that when the cleft is open (Gly-468 is away from the γ-phosphate), the tetrahedral is preferred over the trigonal bipyramidal configuration. In the transition state for hydrolysis ($MgADP{\cdot}VO_4^-$ bound to the active site), the $P_\gamma-O-N_\zeta$ angle becomes significantly larger, viz., 130° (right, Figure 5). In contrast, the $P_\beta-O-N_\zeta$ angle of the same Lys-183 remains essentially constant during the same transit (111° vs 114°). As cited earlier (Figure 3B), the main chain amide nitrogen ($N_{\text{main chain}}$) of Gly-468 creates an interaction with oxygen (3) of the γ-phosphate during the transit to the transition state. The $P_\gamma-O-N_{\text{main chain}}$ angle of Gly-468 was 131°, essentially the same as the new $P_\gamma-O-N_\zeta$ angle of Lys-183. This circumstance suggests a reason why interaction of Gly-468 with the γ-phosphate energetically disposes γ-phosphate to leave from the bridging oxygen between β- and γ-phosphates, and at the same time changes its configuration. If this speculation is granted, several observations are conveniently explained, e.g., why the trigonal bipyramidal configuration is observed only in structures in which the cleft is closed (*5*, *6*), why the K183A[5] system can catalyze hydrolysis even though Lys-183 is involved in the catalysis (unpublished observations), and why, as earlier observed (*1*), the G468A system exhibits neither steady-state ATPase nor an initial phosphate burst.

"Two-Water" Hypothesis of How Myosin Catalyzes ATPase. As described in the foregoing section, w_1 is now oriented to carry out its attack on the γ-phosphate, and, on the other side, the γ-phosphate is readied for the attack from w_1 by changing its configuration into a trigonal bipyramidal. Now, we deal with the question of how hydrolysis proceeds to produce P_i and ADP. No crystal structure of the posthydrolysis state is available, but we can make some guesses about the passage from the transition state to the posthydrolysis state. Our proposal resembles catalysis by the GTPase system. Coleman and Sprang (*9*) have reviewed the latter system, explaining the participation of highly conserved Gln and Arg (in $G_{i\alpha}$, Gln-204 and Arg-178). In our hypothesis, Glu-470—w_2—Gly-468 and Asn-242, respectively, play analogous roles. The essential transformations are depicted in Figure 6. On the left is the transition state, and on the right is a state resulting from hydrolysis. When the γ-phosphate approaches, w_1 splits, the resulting hydroxyl moiety attacks the γ-phosphate (to form P_i), and the resulting proton transfers to w_2 (to form H_3O^+). The positive charge developed at w_2 is stabilized by both the carboxyl group of Glu-470 and the main chain carbonyl oxygen of Gly-468, both of which are negatively charged (denoted as δ^-). After P_i leaves, the terminal oxygen atom of the β-phosphate group of ADP is also ionized. This negative charge is neutralized by the side chain of Asn-242 ($N_{\delta 2}$) and the main chain amide of Gly-180, both of which are positively charged (denoted as δ^+). This model is consistent with crystallographic observations suggesting that Asn-242 and Gly-180 both interact with the bridging oxygen atom of the β-phosphate (*5*, *6*), and also harmonizes with our results that in the N242A system both steps of $M^{**}{\cdot}ADP{\cdot}P_i \rightarrow M^{*}{\cdot}ADP + P_i$ and the displacement of $M^{*}{\cdot}ADP$ are 10 times faster than in the wild-type system (unpublished observations). Our proposal thus resolves the long-standing conundrum about how catalysis seems to be carried out absent an obvious hydrogen acceptor.

Earlier kinetic studies have shown that per mole of ATP hydrolyzed at pH 8.0, one mole of protons is produced, at the rate limitation corresponding to P_i release (*12*, *13*, *26*). Because protons in water exist as hydronium ions, the appropriate chemical equation is

$$ATP^{4-} + Mg^{2+} + 2H_2O \rightarrow ADP^{3-} + Mg^{2+} + HPO_4^{2-} + H_3O^+$$

It seems important that our hypothesis accounts stoichiometrically for each of the chemical species in this equation. These kinetic studies have also shown that for the enzyme-bound system, the equilibrium constant for hydrolysis is near to unity (*12*, *13*, *26*), so it is plausible to assume that at this stage there is a rapid interconversion between similarly weighted structures and thus to account for how experiments in $H_2{}^{18}O$ yield ^{18}O-labeling of more than one per mole (*27*—*29*). This feature of the catalysis may or may not bear on

[5] A mutant is represented by a one-letter expression of the original amino acid residue prior to its sequence number, and that of the mutated residue following to its number, i.e., R183A, G468A, and N242A.

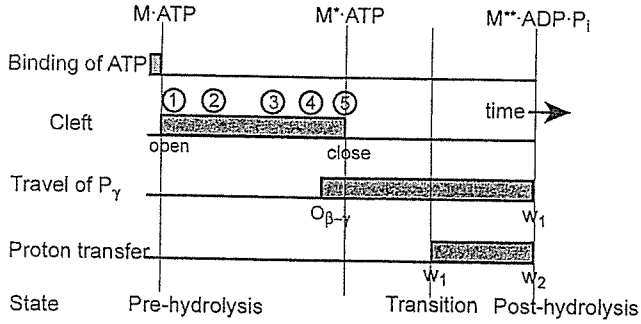

FIGURE 7: A chronological sequence of events during ATP hydrolysis. The period of each event is shown as a gray zone. 1, 2, 3, 4, and 5 represent coordination of Asp-465 to Mg^{2+} via w_3, Ramachandran angle changes at Ile-466, Ala-467, and Gly-468, hydrogen-bonding of Gly-468 to an oxygen of the γ-phosphate, trapping of w_2 between Gly-468 and Glu-470, and salt-bridge formation between Glu-470 and Arg-247, respectively.

how excess labeling of P_i is interpreted. It is conceivable that although the crystallographically observed number of water molecules inside of the cleft is small, the actual number of water molecules in free exchange with the cleft may be large. In that case, the usual mechanism (interconversion and randam labeling) can be invoked.

The name that we use for our proposal stems from our thinking that, in essence, two contiguous water molecules are involved in catalysis, i.e., one becomes the lytic water and the other is the proton acceptor. However, as we have attempted to show, this simplification is embedded in a program of complicated, well-coordinated processes that together constitute "myosin catalysis". Some tracks in time are shown in Figure 7. If we commence a myosin cycle with the binding of ATP to an empty active site (forming of M·ATP), we must think of the cleft closing, which is followed by two processes. One is hydrogen-bonding of the main chain nitrogen atom of Gly-468 to an oxygen atom of the γ-phosphate (denoted as 3 in Figure 7), which affects the choice of the γ-phosphate configuration. As a result, the γ-phosphorus begins its long travel from the $\beta-\gamma$ bridging oxygen to w_1; in other words, inversion of the γ-phosphate begins. Other processes following cleft closing are Arg-247 and Glu-470 forming of the salt-bridge (denoted as 5 in Figure 7), trapping of w_2 by its hydrogen-bonding with both Glu-470 and Gly-468, w_1 leaving from the guanidino group of Arg-247, and hydrogen-bonding between w_1 and w_2. Finally, a nucleophilic attack of w_1 on the γ-phosphate, coupled with the proton transfer from w_1 to w_2, occurs to produce P_i and H_3O^+.

While plausible variants of the "two-water" idea are conceivable, as are elaborations of the role of Lys-183 (*30*, *31*), such a variant must contend with the experimental fact that the mutated system with alanine in place of lysine still accomplishes hydrolysis. Also, any variant must explain why it is necessary to have glutamic acid at 470 to accomplish hydrolysis.

ACKNOWLEDGMENT

We are grateful to Professor H. M. Martinez for his helpful counsel and Professors I. Rayment and D. McKay for significant improvements in our manuscript.

REFERENCES

1. Onishi, H., Morales, M. F., Kojima, S., Katoh, K., and Fujiwara, K. (1997) Functional transitions in myosin: role of highly conserved Gly and Glu residues in the active site. *Biochemistry 36*, 3767−3772.
2. Onishi, H., Kojima, S., Katoh, K., Fujiwara, K., Martinez, H. M., and Morales, M. F. (1998) Functional transitions in myosin: formation of a critical salt-bridge and transmission of effect to the sensitive tryptophan. *Proc. Natl. Acad. Sci. U.S.A. 95*, 6653−6658.
3. Onishi, H., Ohki, T., Mochizuki, N., and Morales, M. F. (2002) Early stages of energy transduction by myosin: roles of Arg in switch I, of Glu in switch II, and of the salt-bridge between them. *Proc. Natl. Acad. Sci. U.S.A. 99*, 15339−15344.
4. Rayment, I., Rypniewski, W. R., Schmidt-Bäse, K., Smith, R., Tomchick, D. R., Benning, M. M., Winkelmann, D. A., Wesenberg, G., and Holden, H. M. (1993) Three-dimensional structure of myosin subfragment-1: a molecular motor. *Science 261*, 50−58.
5. Fisher, A. J., Smith, C. A., Thoden, J. B., Smith, R., Sutoh, K., Holden, H. M., and Rayment, I. (1995) X-ray structures of the myosin motor domain of *Dictyostelium discoideum* complexed with MgADP.BeFx and MgADP·AlF_4^-. *Biochemistry 34*, 8960−8972.
6. Smith, C. A., and Rayment, I. (1996) X-ray structure of the magnesium(II)·ADP·vanadate complex of the *Dictyostelium discoideum* myosin motor domain to 1.9 Å resolution. *Biochemistry 35*, 5404−5417.
7. Dominguez, R., Freyzon, Y., Trybus, K. M., and Cohen, C. (1998) Crystal structure of a vertebrate smooth muscle myosin motor domain and its complex with the essential light chain: visualization of the pre-power stroke state. *Cell 94*, 559−571.
8. Houdusse, A., Kalabokis, V. N., Himmel, D., Szent-Györgyi, A. G., and Cohen, C. (1999) Atomic structure of scallop myosin subfragment S1 complexed with MgADP: a novel conformation of the myosin head. *Cell 97*, 459−470.
9. Coleman, D. E., and Sprang, S. R. (1999) Reaction dynamics of G-protein catalyzed hydrolysis of GTP as viewed by X-ray crystallographic snapshots of $G_{i\alpha1}$. *Methods Enzymol. 308*, 70−92.
10. Coleman, D. E., Berghuis, A. M., Lee, E., Linder, M. E., Gilman, A. G., and Sprang, S. R. (1994) Structures of active conformations of $G_{i\alpha1}$ and the mechanism of GTP hydrolysis. *Science 265*, 1405−1412.
11. Sondek, J., Lambright, D. G., Noel, J. P., Hamm, H. E., and Sigler, P. B. (1994) GTPase mechanism of Gproteins from the 1.7-Å crystal structure of transducin α-GDP-AIF^-_4. *Nature 372*, 276−279.
12. Bagshaw, C. R., and Trentham, D. R. (1974) The characterization of myosin-product complexes and of product-release steps during the magnesium ion-dependent adenosine triphosphatase reaction. *Biochem. J. 141*, 331−349.
13. Bagshaw, C. R., Eccleston, J. F., Eckstein, F., Goody, R. S., Gutfreund, H., and Trentham, D. R. (1974) The magnesium ion-dependent adenosine triphosphatase of myosin. Two-step processes of adenosine triphosphate association and adenosine diphosphate dissociation. *Biochem. J. 141*, 351−364.
14. Morita, F. (1967) Interaction of heavy meromyosin with substrate. I. Difference in ultraviolet absorption spectrum between heavy meromyosin and its Michaelis−Menten complex. *J. Biol. Chem. 242*, 4501−4506.
15. Werber, M. M., Szent-Györgyi, A. G., and Fasman, G. D. (1972) Fluorescence studies on heavy meromyosin-substrate interaction. *Biochemistry 11*, 2872−2883.
16. Johnson, W. C., Jr., Bivin, D. B., Ue, K., and Morales, M. F. (1991) A search for protein structural changes accompanying the contractile interaction. *Proc. Natl. Acad. Sci. U.S.A. 88*, 9748−9750.
17. Hiratsuka, T. (1992) Spatial proximity of ATP-sensitive tryptophanyl residue(s) and Cys-697 in myosin ATPase. *J. Biol. Chem. 267*, 14949−14954.
18. Batra, R., and Manstein, D. J. (1999) Functional characterisation of *Dictyostelium* myosin II with conserved tryptophanyl residue 501 mutated to tyrosine. *Biol. Chem. 380*, 1017−1023.
19. Yengo, C. M., Chrin, L. R., Rovner, A. S., and Berger, C. L. (2000) Tryptophan 512 is sensitive to conformational changes in the rigid relay loop of smooth muscle myosin during the MgATPase cycle. *J. Biol. Chem. 275*, 25481−25487.